Applied Energy 384 (2025) 125467

Contents lists available at ScienceDirect

Applied Energy

journal homepage: www.elsevier.com/locate/apenergy

Feasibility study of green ammonia and electricity production via an innovative wind-solar-biomass polygeneration system

Mohammad Hasan Khoshgoftar Manesh [a,*], Soheil Davadgaran [a], Seyed Alireza Mousavi Rabeti [a], Ana M. Blanco-Marigorta [b]

[a] Energy, Environmental and Biological Systems Research Lab (EEBRlab), Division of Thermal Sciences and Energy Systems, Department of Mechanical Engineering, Faculty of Technology & Engineering, University of Qom, Qom, Iran
[b] Department of Process Engineering, Universidad de las Palmas de Gran Canaria, Las Palmas de Gran Canaria, Spain.

HIGHLIGHTS

- A novel solar-biomass-wind driven polygeneration system is presented.
- power, process steam, and ammonia are the productions of the proposed system.
- The machine learning approach is used to model the system's performance.
- The optimal payback period of the proposed system is estimated at 3 years.
- The optimal total environmental impact rate for the system is calculated at 48.98 Pts/hr.

GRAPHICAL ABSTRACT

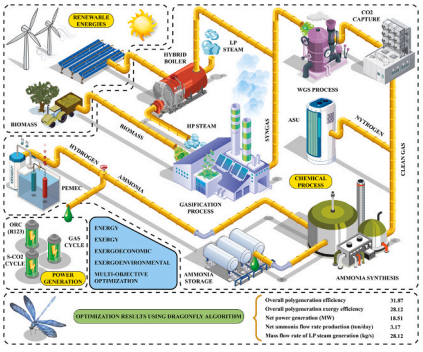

ARTICLE INFO

Keywords:
4E analysis
Polygeneration
Optimization
Solar-Biomass-Wind
Ammonia

ABSTRACT

The increase in greenhouse gases in the world due to the use of fossil fuels and the risk of losing non-renewable resources are important factors in the expansion of renewable polygeneration systems. The current research focuses on integrating solar-biomass-wind renewable energies to produce power, process steam, and ammonia simultaneously. The general operation of the proposed system is that a syngas-solar hybrid boiler is used to produce steam at two low-pressure and medium-pressure levels. Medium-pressure steam has been used as the feed of gasification process unit along with air and municipal solid waste. The syngas produced from the gasification unit is used to supply boiler fuel and ammonia unit feed. Before the ammonia synthesis process, it is necessary to purify the feed syngas. In this regard, water gas shifting and CO_2 capture units have been used for purification. Next, the purified syngas with nitrogen in the presence of ammonia synthesis reactors are converted to ammonia. The nitrogen feed needed by the unit is created through a cryogenic air separation unit that supplies its electricity from wind turbines. A part of the ammonia produced has been used to fuel the downstream power generation unit. The Brayton open cycle based on ammonia-hydrogen hybrid fuel uses the described ammonia stream. The hydrogen required by this unit is supplied from the wind PEM electrolyzer. Finally, supercritical carbon dioxide cycles and organic Rankine cycle have been used to recover heat output from the Brayton cycle. Geothermal energy has also been used to preheat the organic fluid entering the turbine to increase power.

* Corresponding author.
E-mail address: m.khoshgoftar@qom.ac.ir (M.H. Khoshgoftar Manesh).

https://doi.org/10.1016/j.apenergy.2025.125467
Received 14 October 2024; Received in revised form 21 December 2024; Accepted 28 January 2025
Available online 13 February 2025

Energy, exergy, exergeoeconomic, and exergoenvironmental (4E) analyses, along with sensitivity analysis and multi-objective optimization using the dragonfly algorithm, were performed. The overall energy efficiency, exergy efficiency, total cost rate, and environmental impact rate were 31.33 %, 38.53 %, 1.56 $/s, and 14.77 mPts/s, respectively. Three-objective optimization improved energy efficiency by 1.72 % and reduced the total cost rate by 15.86 %. In optimal operation, the system produces 275.44 tons/day of ammonia, 3.17 kg/s of steam, and 18.51 MW of power. The payback period was calculated to be 3.29 years, but in real-world scenarios, it may be longer, so the result should be interpreted cautiously.

Nomenclature

A	*Area (m^2)*
AC	*Air Compressor*
ACC	*Air Cooled Condenser*
AF	*Air to Fuel Ratio*
AGT	*Ammonia Gas Turbine*
ANN	*Artificial Neural Networks*
APU	*Ammonia Production Unit*
ASU	*Air Separation Unit*
b	*Environmental Impact per Exergy (Pts/kJ)*
B	*Environmental Impact (Pts)*
C	*Carbon*
c	*Cost per Exergy ($/kJ)*
C	*Cost ($)*
CC	*Combustion Chamber*
Comp	*Compressor*
CRF	*Cost Recovery Factor*
D	*Diameters*
DNI	*Direct Normal Irradiation (W/m^2)*
Ex	*Exergy*
ex	*Specific Exergy (kJ/kg)*
F	*Faraday's constant (C/mol)*
GP	*Genetic Programming*
GT	*Gas Turbine*
h	*Specific Enthalpy (kJ/kg)*
H	*Hydrogen*
HDH	*Humidification-Dehumidification*
HP	*High Pressure*
HX	*Heat Exchanger*
J	*Current Density (A/m^2)*
KNN	*K-Nearest Neighbors*
LCA	*Life Cycle Assessment*
LHV	*Low Heating Value (kJ/kg)*
LP	*Low Pressure*
m	*Mass (kg)*
MC	*Moisture Content*
MED	*Multi-Effect Distillation*
MFC	*Microbial Fuel Cells*
ML	*Machine learning*
MSW	*Municipal Solid Waste*
N	*Nitrogen*
n	*system's lifespan (years)*
N	*Hour of Working System in a year (hour), Mole*
NSGA-II	*Non-dominated Sorting Genetic Algorithm II*
O	*Oxygen*
ORC	*Organic Rankine Cycle*
ORCP	*Organic Rankine Cycle Pump*
ORCT	*Organic Rankine Cycle Turbine*
P	*Pressure (bar), Pump*
PEC	*Purchasing Equipment Cost ($)*
PEM	*Proton Exchange Membrane*
PEMEC	*PEM electrolyzer*
PTC	*Parabolic Through Collectors*
Q	*Heat (kJ)*
R	*Global Gas Constant (kJ/kmol.K)*
RO	*Reverse Osmosis*
s	*Specific Entropy (kJ/kg.K)*
S-CO_2	*Supercritical CO_2*
SHX	*Solar Heat Exchanger*
T	*Temperature (K)*
TIP	*Turbine Inlet Pressure (bar)*
TIT	*Turbine Inlet Temperature (K)*
V	*Velocity (m/s), Volume (m3)*
V	*Overpotential (V)*
W	*Work (kJ)*
WGS	*Water Gas Shifting*
WT	*Wind Turbine*
X	*Mole Fraction*
Y	*Environmental Impact Rate of Equipment(Pts/s)*
y	*Mole Fraction*
Z	*Investment Cost Rate of Equipment ($/s)*

Sub Script

0	*Reference State*
a	*Ambient, Air, Anode*
act	*Activation*
C	*Compressor*
c	*Cathode*
ch	*chemical*
D	*Destruction*
F	*Fuel*
fg	*flue gas*
GF	*Gasification*
in	*Inlet*
k	*Component*
out	*Outlet*
P	*Product*
P	*Pump*
ph	*Physical*
Q	*Heat*
s	*Surface, Isentropic*
SF	*Solar Field*
sg	*Syngas*
T	*Turbine*
u	*Useful*
W	*Work*

Greek Symbols

η	*Efficiency*
ρ	*Density (kg/m^3)*
ϕ	*Maintenance Factor*
ψ	*Exergy Efficiency*

1. Introduction

In the energy sector, there are numerous challenges, including the rise in fossil fuel prices, diminishing oil production, increasing environmental impacts, and global warming [1]. Fossil fuel consumption elevates greenhouse gas emissions, leading to climate changes that significantly affect life globally [2]. Fossil fuels not only contribute to air pollution and respiratory illnesses but also emphasize the growing reliance on natural gas as a transitional energy source, underscoring the urgent need for innovative systems that maximize efficiency while minimizing environmental impacts and accelerating the shift to sustainable renewable energy alternatives [3,4].Improper disposal of waste and reliance on fossil fuels significantly contribute to environmental pollution, emphasizing the need for renewable energy systems and sustainable solutions [5]. Due to its biological characteristics, biofuel production has been introduced as a significant and sustainable option for energy supply. Biofuels, derived from organic materials such as plants and agricultural waste, have emerged as an environmentally friendly substitute for fossil fuels [6]. Unlike fossil fuels, burning biofuels produces fewer pollutants, thus reducing greenhouse gases and improving environmental health [7]. In recent decades, there has been an increasing focus on the use of renewable energies, and with the continuous growth of this energy industry, this attention can further escalate.

One notable example of biofuels is ammonia. Ammonia can be employed as an auxiliary fuel and a substitute for fossil fuels in industries. The combustion of ammonia produces water and nitrogen, which are non-polluting by-products, making it a clean fuel. Ammonia, as a chemical energy carrier, enables the storage of energy produced from renewable sources such as wind and solar. This storage facilitates a stable and continuous energy supply during periods of production fluctuations, thereby enhancing energy security [8]. Additionally, the production of ammonia and its substitution for fossil fuels can lead to a reduction in air pollution, as well as the generation of clean energy [9]. Methods of producing ammonia include synthesizing it from natural gas reforming [10] and producing it using syngas obtained from the gasification process [11,12]. Moreover, ammonia can be considered as a method for hydrogen storage and transportation. Given that hydrogen is not readily available and its storage is a complex and costly process, producing ammonia from the reaction of hydrogen and nitrogen is proposed as an alternative approach [13]. In this regard, Lamb et al. [14] have suggested ammonia as an effective means for hydrogen storage and transport. Ezzat et al. [15] introduced a multigeneration system based on ammonia fuel in their research. This system consists of two main power sources, namely a hydrogen-ammonia gas turbine cycle and a solid oxide fuel cell with ammonia. The results justify the effective use of ammonia as a substitute fuel for fossil fuels. The energy efficiency and exergy efficiency of this system are 58.78 % and 50.66 %, respectively. This emphasizes ammonia's potential not only as a clean fuel but also as a critical component in integrated renewable energy systems. Other renewable energy-based methods for ammonia production are presented in **Table 1**.

Given the numerous advantages that renewable energies offer in the fields of health, economy, and environment, the utilization of these energy sources is highly rational and justifiable [21,22]. Although each renewable energy source brings significant capabilities independently, integrating these types of energies can significantly improve energy efficiency and reduce production costs [23,24]. The integration of solar, biomass, wind, and wave technologies has been shown to reduce greenhouse gas emissions by up to 93 % in certain configurations [25]. Combining biomass gasification with solar photovoltaic energy has proven to be an effective solution for providing sustainable electricity in rural regions [26]. Recent studies emphasize this integration, highlighting effective systems for clean energy production [27,28]. This integration of renewable energies, such as in Power-to-X strategies, has been shown to significantly reduce CO_2 emissions and enhance exergy

Table 1
Comparison of renewable energy-based ammonia production methods.

Method of Production	Renewable Energy Source	Method Description	Advantages	Disadvantages	Ref.
Electrolytic Ammonia Production	Wind Solar	This method involves the electrolysis of water to produce hydrogen, which is then combined with nitrogen to produce ammonia.	- Reduces greenhouse gas emissions - Utilizes green hydrogen - Compatible with renewable energy grids	- Requires hydrogen storage - High electrolysis costs	[16]
Biomass-Based Ammonia Production	Biomass	In this method, agricultural waste or other biomass sources are converted to hydrogen and then to ammonia.	- Utilizes agricultural waste - Produces sustainable hydrogen - Reduces reliance on fossil fuels	- Lower efficiency compared to other methods - High biomass supply costs	[17]
Solar Energy Ammonia Production	Solar	This method uses solar energy to produce hydrogen through high-temperature electrolysis in a solid oxide electrolyzer cell (SOEC). The hydrogen is then combined with nitrogen to synthesize ammonia.	- No reliance on fossil fuels - Unlimited solar energy - Reduces long-term energy costs	- Requires extensive land for solar panels - Dependent on sunlight	[18]
Wind Energy Ammonia Production	Wind	In this method, wind energy is used to generate electricity, and ammonia is produced and stored as an energy carrier to balance the intermittent nature of wind energy.	- Utilizes a stable energy source - Reduces air pollution - Enhances energy diversity	- Production instability due to wind variability - High installation and maintenance costs	[19]
Combined: Solar-Wind	Wind Solar	This method integrates wind and solar energy as simultaneous sources for ammonia production.	- Optimizes the use of energy resources - Increases stability and reliability - Reduces overall energy costs	- High installation and operational costs - Requires energy storage systems	[20]

efficiency [29]. Mousavi Rabeti et al. [30] demonstrated that integrating solar and biomass renewable energies in a polygeneration system for power, heat, freshwater, and hydrogen production can be highly effective. The examination of this system was conducted using municipal solid waste (MSW) as the biomass source. The results indicated that the overall energy efficiency and exergy efficiency are 39 % and 32.01 %, respectively. Furthermore, the integration of renewable energies can enhance flexibility and increase reliability in product manufacturing. Hybrid systems combining solar energy with energy storage technologies have shown significant potential in achieving sustainable freshwater production [31,32]. Mehrabian et al. [33] presented a polygeneration system based on wind, solar, and biomass renewable energies for producing hydrogen, oxygen, and distilled water. The results of integrating these renewable energies led to a reduction in environmental impacts and the production of the required power for PEM electrolyzer (PEMEC). In a study conducted by Bersalli et al. [34] in Europe and Latin America, the results indicated that the utilization of renewable energies can significantly reduce energy production costs. Khani et al. [35] presented a solar-based polygeneration system. The proposed system is designed to provide electricity, freshwater, and the required carbon dioxide for the greenhouse. Results indicate that this integration increases the efficiency of ORC power generation from 37.3 % to 59.41 %. Numerous studies have been conducted in the field of renewable energy integration in recent decades to increase energy efficiency, and various solutions have been proposed. Similar multi-generation systems have been studied in different global regions, demonstrating economic feasibility in diverse contexts [31].

One of the practical methods for integrating energy systems and achieving valuable products is through polygeneration and cogeneration systems [36]. These systems can simultaneously produce value-added products using various energy sources, both renewable and fossil. These systems, when utilizing biogas and methane, demonstrate improved energy efficiency and environmental performance [37]. They utilize multiple subsystems, leading to increased energy efficiency, reduced emissions, cost savings, and decreased thermal losses [38]. **Table 2** illustrates recent studies on polygeneration systems that utilize

Table 2
A summary of studies conducted in the field of renewable energy in modern polygeneration systems.

Authors	Year	Energy sources	Products	Analysis results	Subsystems
Khoshgoftar Manesh et al. [45]	2024	Biomass Solar Wind	Power Freshwater Ammonia	Exergy efficiency = 13.12 % Energy efficiency = 29.97 %	Hybrid boiler Ammonia synthesis unit Hydrogen-ammonia gas cycle S-CO_2 cycle ORC (R123) MED HDH
Ghasemi et al. [46].	2024	Biomass Solar	Power Hydrogen Freshwater	Exergy efficiency = 32.2 % Energy efficiency = 38.8 %	Linear Fresnel concentrator -driven solar farm Gasification Alkaline water electrolyzer MED ORC (R141B)
Khoshgoftar Manesh et al. [47]	2024	Solar Wind	Power Freshwater	Exergy efficiency = 4.55 % Energy efficiency = 22.09 %	Microbial desalination cell (MDC) HDH RO
Shariati et al. [48].	2024	Biomass Fossil fuel	Cooling load Hot water Power	Exergy efficiency = 35 % Energy efficiency = 78 %	Gasification and combustion chamber Double-effect absorption chiller S-CO_2 cycle
Mousavi Rabeti et al. [49].	2023	Solar Biomass	Power Freshwater Heat Hydrogen Oxygen Carbon dioxide Methanol	Exergy efficiency = 23.59 % Energy efficiency = 29.25 %	Gasification Kallina cycle Brayton cycle Double-pressure steam cycle RO desalination MED MFC ORC
Hajimohammadi Tabriz et al. [50].	2023	Urban sewage Biomass	Power Hydrogen, Freshwater Heating	Exergy efficiency = 40.18 % Energy efficiency = 35.48 %	Brayton cycle Atmospheric water harvesting Steam Rankine cycle ORC Gasification Hydrogen production unit
Hashemian and Noorpoor [51]	2022	Biomass Geothermal	Power Hydrogen Oxygen Freshwater Cooling Heating	Exergy efficiency = 16.45 % Energy efficiency = 58.54 %	Rankine cycle Dual-effect absorption refrigeration PEMEC Biomass combustor MED
Safder et al. [52].	2021	Biomass	Power Freshwater Cooling	Exergy efficiency = 77.49 % Energy efficiency = 92.10 %	Brayton cycle Rankine cycle Kalina cycle Ejector refrigeration cycle MED
Ghasemiasl et al. [53].	2021	Solar Fossil fuel	Electricity Freshwater	Exergy efficiency = 49.64 % Energy efficiency = 57.36 %	ORC Brayton cycle MED PEMEC
Ehyaei et al. [54].	2021	Geothermal	Electricity Potable water Hydrogen Cooling energy Salt	Exergy efficiency = 19.6 % Energy efficiency = 12.25 %	Goswami cycle RO Sodium hypochlorite plant

different subsystems. As indicated in **Table 2**, polygeneration systems can produce products such as freshwater, power, ammonia, cooling, and hydrogen [4]. The economic and environmental characteristics of these systems are crucial, making the selection of appropriate subsystems highly significant. Solar-assisted systems, particularly those that integrate multiple energy sources, demonstrate significant improvements in both energy efficiency and economic performance [39]. Common subsystems include the Brayton cycle, supercritical carbon dioxide cycle (S-CO_2 cycle), organic Rankine cycle (ORC), desalination units, and gasification units. In the Brayton cycle, fuels such as methane, hydrogen, biogas, and ammonia can be used for power and heat generation [40]. The goal is to reduce negative environmental impacts from fossil fuels [41]. The S-CO_2 cycle operates using carbon dioxide in a supercritical state as the working fluid in a closed-loop system. This method offers advantages over traditional steam-based power cycles, including increased efficiency and reduced greenhouse gas emissions [42]. Hajimohammadi Tabriz et al. [43] introduced a cost-effective polygeneration system based on biomass for hydrogen production from municipal sewage sludge. Their system includes subsystems such as the Brayton cycle, water gas shift reaction, biomass conversion, and atmospheric water harvesting, achieving exergy and energy efficiencies of 38.26 % and 35.24 %, respectively. Wang et al. [44] proposed a polygeneration system for recovering waste heat in coal-fired power plants, producing power, desalinated wastewater, and space cooling. This system comprises ORC, Humidification-Dehumidification (HDH), and a desiccant cooling system. Machine learning (ML) enhances the integration and analysis of energy systems in polygeneration applications.

Recently, with the increasing efficiency of energy systems, the application of machine learning (ML) has expanded in this field. This technology plays a crucial role in improving performance, reducing costs, and enhancing system flexibility [55]. One significant advantage of ML is its ability to extract governing relationships within energy systems. These relationships eliminate the need for complex equations in system analysis, significantly increasing computation speed. To derive these governing equations, data related to the energy system under investigation must be collected. This data typically includes temperature, pressure, volume, and other relevant thermodynamic variables. To achieve accurate models, heterogeneous data is filtered out, and ML algorithms are then employed to create predictive models for the energy system. The accuracy of these relationships is subsequently measured. Another application of ML is optimizing energy systems by utilizing various algorithms [56]. Common algorithms include decision trees, support vector machines, artificial neural networks (ANN), and more advanced techniques like convolutional neural networks, which offer higher accuracy. Khoshgoftar Manesh et al. [57] extracted high-precision relationships for gasification using thermodynamic data from municipal solid waste (MSW) gasification. They employed deep ANN algorithms combined with genetic programming (GP). Ghasemzadeh et al. [58] introduced a biogas-based power plant optimized using ML methods and the grey wolf optimization algorithm. Ghandehariun et al. [59] successfully predicted the exergy efficiency of their proposed system using the Backpropagation Neural Network algorithm, achieving an R-squared value of 0.98, which demonstrates high accuracy. It is important to note that ML and energy systems optimization enable quicker decision-making, leading to increased efficiency.

Given the importance of energy resources, which are limited in accessibility, along with the need to reduce production costs and environmental impacts, optimization in energy systems is an appropriate solution [60]. This optimization primarily aims to achieve multiple objectives simultaneously, some of which involve minimizing certain factors while maximizing others. This approach is referred to as multi-objective optimization [61]. Objectives can include increasing efficiency, reducing costs, decreasing pollutant emissions, and increasing product output [62]. Various algorithms are employed for optimization in energy systems, including the grey wolf optimization algorithm, salp swarm algorithms, and genetic algorithms [63]. Liu et al. [64] introduced a polygeneration system for generating cooling, power, and freshwater, utilizing the non-dominated sorting genetic algorithm II (NSGA-II) for optimizing system performance. Their results indicated total output power, cooling capacity, and freshwater production of 273.769 kW, 12.997 kW, and 24.23 g/s, respectively. Mahmoudan et al. [65] focused on achieving optimal performance by adopting two parameters: maximum exergy efficiency and minimum total product costs. Their system included parabolic trough collectors, a Kalina cycle, an ejector refrigeration system, a thermoelectric generator unit, ORC, and a PEM electrolyzer for producing cooling load, hydrogen, electricity, and domestic hot water. Through multi-objective optimization with the NSGA-II algorithm, they achieved exergy efficiency of 35.2 % and total product costs of 37.8 $/GJ. Emphasizing the importance of optimizing energy systems leads to better management of energy resources, enhancing the efficiency of proposed systems.

Review studies indicate that interest in using renewable energy for polygeneration systems has increased. Optimizing these systems is crucial for reducing costs and enhancing efficiency. Some energy systems require complex mass and energy balance relationships for modeling, making this process difficult and time-consuming. One effective approach to analyze these systems is linking specialized commercial software with coding software, facilitating the creation of optimization problems. A promising solution to this challenge is the use of machine learning, which has received limited attention from energy systems researchers. Therefore, in the present work, a novel solar-biomass-wind polygeneration system is analyzed in terms of energy, exergy, exergeoeconomic, and exergoenvironmental metrics using machine learning. The innovative renewable polygeneration system produces power, ammonia, and process steam. The power generation components are integrated from wind turbines, Brayton cycle, supercritical carbon dioxide cycle, and organic Rankine cycle. The application of machine learning in the gasification unit, ammonia synthesis unit, and air separation unit has reduced the modeling computation time. Additionally, the use of AI in optimizing solar cogeneration systems has resulted in exergy efficiencies of up to 36.44 % and cost rates of 13.76 $/hour [66]. Finally, three-objective and four-objective optimization of the proposed system has been conducted using the multi-objective dragonfly algorithm. The modeling and analysis are the results of integrating multiple software for the proposed system, culminating in a comprehensive code developed in MATLAB software. Integrating renewable energy systems with advanced technologies like machine learning further enhances system performance and sustainability [67]. The complexity of the proposed system arises from the necessity to efficiently utilize both the chemical and thermal energy contained in syngas while producing multiple valuable outputs, including electricity, ammonia, and process steam. Syngas derived from biomass serves as a versatile energy carrier with the potential to be converted into ammonia—a clean fuel and a widely used industrial product. Furthermore, instead of wasting the thermal energy generated from syngas combustion, it is recovered through heat recovery cycles such as SCO_2 and ORC, which significantly enhance the overall system efficiency and minimize energy losses. This approach not only prevents energy waste but also substantially improves the system's flexibility and overall performance. The innovations and measures implemented in this work are as follows:

1. Presentation of a novel solar-biomass-wind polygeneration system
   This study proposes a novel renewable-driven polygeneration system for the production of power, process steam, and ammonia. The integration of solar energy, biomass, wind, and geothermal energy is achieved through a solar parabolic trough collector field, an air-steam gasification section, a wind turbine farm, and a geothermal heat exchanger, respectively. A solar-syngas hybrid boiler produces process steam, while an ammonia synthesis unit based on syngas and nitrogen feeds is used for ammonia production. Power generation is facilitated by a combination of ammonia-hydrogen Brayton cycle,

supercritical carbon dioxide cycle, and organic Rankine cycle. Nitrogen and hydrogen in the proposed polygeneration system are generated by an air separation unit and PEM electrolyzer, respectively.

2. Machine learning application for analyzing sections of the proposed polygeneration system

   A combination of genetic programming and machine learning is employed to model the gasification section, ammonia synthesis unit, and air separation unit, increasing the modeling speed of the proposed system.

3. 4E analysis, sensitivity analysis, and multi-objective optimization of the proposed system

   A comprehensive energy, exergy, exergoeconomic, and exergoenvironmental (4E) analysis, along with sensitivity analysis, has been performed for the presented study. Additionally, multi-objective optimization based on the multi-objective dragonfly algorithm is utilized to enhance the performance of the proposed polygeneration system.

2. System description

The present work proposes a polygeneration system utilizing renewable energy sources, including solar, wind, geothermal, and biomass, to produce ammonia, power, and heat (as process steam). This system is designed for Tehran, Iran, with geographical coordinates of 51.33° E longitude and 35.72° N latitude. The average direct normal irradiance (DNI) and wind speed in this region are 514.05 W/m^2 and 4.5 m/s, respectively [68]. The geothermal source provides heat up to a maximum temperature of 110 °C. The biomass used in the gasification process is municipal solid waste (MSW), with an average production rate of 2 million tons/year. The input values for modeling the proposed polygeneration system are presented in Table 3.

The system includes the following subsystems: gasification process, water gas shift process, CO_2 capture, ammonia synthesis, hydrogen-ammonia gas cycle, supercritical CO_2 (S-CO_2) cycle, and ORC (R123). Fig. 1 illustrates a schematic of the designed system. The process begins with steam generation for the gasification process. For steam generation at two pressure levels, low pressure (LP) and high pressure (HP), a hybrid boiler using solar energy and syngas is employed. Water enters the boiler (stream 2), is preheated by syngas combustion heat, and exits from stream 4. Solar energy is used to improve steam production efficiency and reduce water latent heat loss. Water exchanges heat at two levels with parabolic trough collectors (PTC), and LP steam exits from stream 8 while HP steam exits from stream 16. The LP steam is used as process steam, and HP steam, along with air and MSW, enters the gasifier for syngas production. ET-100 model PTCs are used [69]. The chemical reaction in the gasifier is presented below.

$$CH_\alpha O_\beta N_z + wH_2O + m(O_2 + 3.76N_2) \rightarrow x_1H_2 + x_2CO + x_3CO_2 + x_4H_2O + x_5CH_4 \quad (1)$$

Some of the produced syngas is utilized as fuel in the hybrid boiler, while the remaining portion (stream 21) enters the expander for power generation due to its high temperature and pressure. The syngas contains carbon monoxide, carbon dioxide, nitrogen, and hydrogen. To produce ammonia with high efficiency, syngas must be free of carbon monoxide and carbon dioxide. Therefore, the syngas is introduced to the water gas shift (WGS) process to convert CO to CO_2 through reaction with water. To ensure complete conversion of CO to CO_2 and maximize the efficiency of hydrogen production, the proposed system employs a two-stage water WGS process. This dual-reactor configuration ensures that over 99.5 % of the CO is converted, leaving the syngas highly purified and suitable for downstream ammonia synthesis. The reaction relevant to the WGS is shown in eq. 2.

$$CO + H_2O \longleftrightarrow CO_2 + H_2 \quad (2)$$

Table 3
The main inputs of different parts of the proposed polygeneration system for modeling.

Parameters	Unit	Value	Parameters	Unit	Value
Biomass (MSW) [57]			**PTC**		
Moisture content	%	10	Pinch point of HX	°C	50
Carbon	%	51.03	TTD of HX	°C	30
Hydrogen	%	6.77	PTC outlet pressure	bar	3
Oxygen	%	39.17	Pressure drop of PTC	%	15
Nitrogen	%	2.64	PTC Field 1 parallel collectors	–	7
Steam Boiler			PTC Field 2 parallel collectors	–	15
Pump isentropic efficiency	%	80	**Expander**		
Boiler inlet pressure	bar	3	Expander outlet pressure	bar	4.50
LP steam outlet	bar	2	Expander isentropic efficiency	%	90
Pressure drop in HX	%	2	**Wind Turbine (WT) [72]**		
Mass flow rate of LP steam	Kg/s	5	Average wind speed	m/s	4.80
Boiler efficiency	%	90	Average WT installation height	m	10
AFR in boiler	–	3.50	Number of WTs	–	35
ASU			Tower height	m	85
Output Nitrogen pressure	bar	12	Hub height	m	80
Output Oxygen pressure	bar	12	Blade length	m	76.60
PEMEC [74]			Power coefficient	%	44
PEMEC pressure	bar	1	Ground surface	–	0.15
PEMEC temperature	°C	80	**Hydrogen-Ammonia Gas Cycle [15]**		
Anode activation energy	j/mol	76,000	GT pressure ratio	–	13
Cathode activation energy	j/mol	18,000	AC isentropic efficiency	%	90
Anode membrane water content	1/Ω	14	GT isentropic efficiency	%	92
Cathode membrane water content	1/Ω	10	TIT	°C	1291
Membrane thickness	m	1×10^{-4}	GT net power	MW	15
Anode current density	A/m^2	1.7×10^5	**S-CO_2 Cycle [75]**		
Cathode current density	A/m^2	4.6×10^3	Compressor inlet temperature	°C	36.85
Anode exchange current density	A/m^2	1×10^{-5}	Compressor inlet pressure	bar	87.20
Cathode exchange current density	A/m^2	10	TIT	°C	378.90
ORC [76]			TIP	bar	273.20
TIT	°C	123	Turbine isentropic efficiency	%	90
TIP	bar	12.01	Compressor isentropic efficiency	%	85
Condenser pressure	bar	1.55	HX effectiveness	%	60
OFOH pressure	bar	5.81	Hot side pressure drop in HX	bar	0.42
Geothermal inlet pressure	bar	10	Cold side pressure drop in HX	bar	1.40
ORCP's isentropic efficiency	%	75	Pinch temperature of S-CO_2 HX	°C	20
ORCT's isentropic efficiency	%	85	**Gasification process**		
HX ΔT	°C	10	Gasification pressure	bar	9
Cooling air ΔT	°C	10	Syngas mass flow rate	Kg/s	50
Geothermal inlet temp	°C	110	AC isentropic efficiency	%	80
ORC-Geothermal HX ΔT	°C	10			
Geothermal outlet temperature	°C	90			

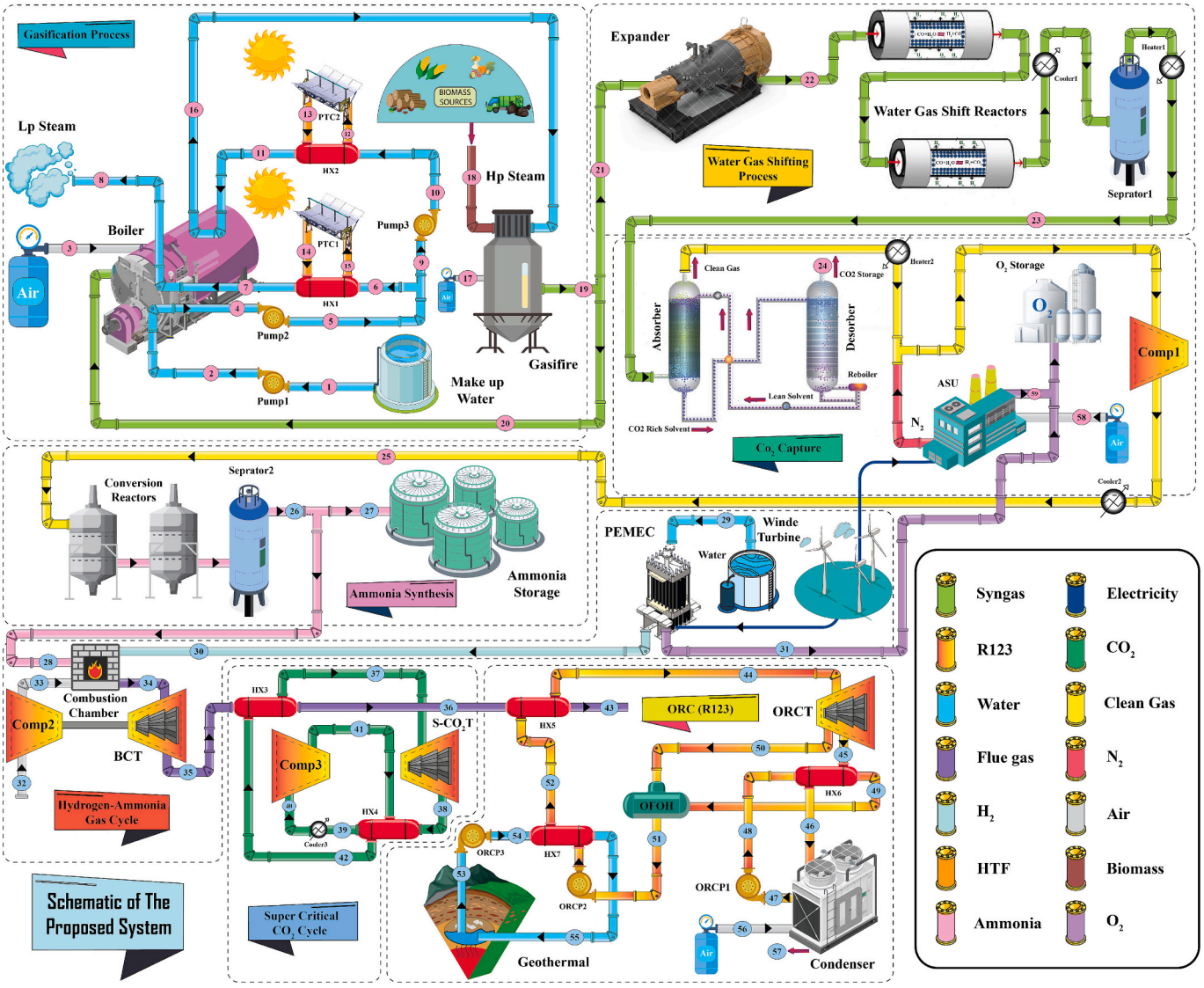

Fig. 1. Schematic of polygeneration system based on solar, wind, geothermal and biomass renewable energy to produce ammonia, power and heat.

After passing through the WGS reactors, the syngas is free of CO. Next, CO_2 is absorbed in the CO_2 capture unit, and nitrogen is injected. Since the nitrogen content in syngas is insufficient to react with all available hydrogen for ammonia production, additional nitrogen is added from the air separation unit (ASU). The enriched gas with nitrogen and hydrogen enters the ammonia synthesis stage, where the reaction takes place in two reactors at 350 °C and 30 bar with a fractional conversion of 25 % [70,71]. In the proposed system, the removal of CO and CO_2 is achieved through a meticulously designed multi-stage process to ensure that the syngas meets the stringent purity requirements for ammonia synthesis. The WGS reactors converts over 99 % of CO into CO_2, and advanced separation techniques subsequently capture more than 99.5 % of the CO_2. To address any residual amounts, final purification steps utilizing advanced catalytic beds or additional adsorption techniques are implemented. As clearly stated in the System Description section, the syngas after these processes is entirely free of CO and CO_2. This ensures that there is no risk of catalyst poisoning during the ammonia synthesis process, and the system fully complies with the industrial standards required for downstream catalytic operations. The ammonia production reaction is shown in eq. 3.

$$N_2 + 3H_2 \leftrightarrow 2NH_3 \quad (3)$$

High-purity ammonia is separated in the separator. A portion of this ammonia is stored for economic purposes and backup support, while another portion is used in the hydrogen-ammonia gas cycle. At this stage, ammonia, along with hydrogen produced by the proton exchange membrane electrolyzer (PEMEC), is transferred to the combustion chamber of the ammonia-hydrogen gas cycle. Hydrogen is added to increase the lower heating value (LHV) of the fuel. The power required for PEMEC and ASU operation is supplied by renewable wind energy, using the LTW77 wind turbine model with a capacity of 1 MW [72]. To reduce losses and recover heat, the system also utilizes the S-CO_2 cycle and ORC for power generation. The working fluid in the ORC is R123, while geothermal energy is used in the S-CO_2 cycle to provide the required heat for the cycle. R123 has been selected as the working fluid in the ORC due to its high thermal efficiency and low global warming potential (GWP). Its favorable thermodynamic properties allow for effective operation under the specific conditions of our system. Additionally, R123's stability at elevated temperatures enhances the overall reliability and performance of the energy conversion process. It should be noted that, the hybrid boiler, which integrates syngas combustion with solar energy, plays a key role in improving steam production efficiency while reducing energy losses. A critical innovation of the proposed polygeneration system is the integration of the S-CO_2 and ORC cycles to maximize energy recovery and boost overall efficiency. The S-CO_2 cycle effectively recovers thermal energy at medium-to-high

temperature levels due to its superior thermodynamic properties, such as high density and excellent heat transfer capability. In tandem, the ORC cycle operates efficiently at lower temperatures, ensuring that waste heat from the Brayton cycle (ammonia-hydrogen combustion) and the hybrid boiler is fully utilized instead of being lost. This innovative combination ensures comprehensive heat recovery across all temperature ranges, significantly improving system performance and addressing energy losses. Moreover, the design enhances system flexibility by enabling efficient energy management during peak power demand. The recovered heat not only increases power generation but also strengthens the system's resilience, making it a reliable and sustainable solution for multi-generation applications.

Assumptions used in the proposed system:

- The system is considered in a steady state, and kinetic and potential energies are neglected in all streams.
- Adequate time is available for the gasification reaction, so this process is assumed to be at equilibrium, and a constant gasification pressure is considered [73].
- Additionally, the production of tar, char, nitrogen oxides, sulfur, chlorides, etc., in the syngas products is disregarded [73].
- Heat losses in all heat exchangers are neglected.
- The operating temperature and pressure of the water gas shift (WGS) reactors are assumed to be 450 °C and 14.4 bar, respectively, with a fractional conversion of 88.2 % [70].
- The temperature and pressure in the PEMEC are assumed to be constant and equal to 80 °C and 1 bar, respectively [74].

In energy systems, mass accumulation is disregarded due to the inherent nature of these systems, making the assumption of a steady state logical and correct. Neglecting kinetic and potential energies in the streams is also logical since their values are small and do not significantly impact the system's performance. Since the objective is to assess the feasibility of the proposed system, disregarding these parameters does not introduce major errors.

The gasification process, although kinetic in nature, is often modeled using an equilibrium assumption for simplicity. Studies by Mousavi Rabeti et al. [30] have shown that results obtained from this assumption are comparable to experimental data, with minimal differences. Since the focus of this work is not on detailed gasification analysis, the equilibrium assumption is valid [73]. Additionally, by assuming equilibrium, reaction rate changes are disregarded, and gasification is considered to occur at constant pressure [73].

The production of minor syngas components such as tar, char, nitrogen oxides, sulfur, and chlorides is disregarded for simplicity. Including these components would require considering their equilibrium constants, which is complex and costly. Given their low composition in the gas mixture, their omission does not significantly affect the results [73].

Heat loss in the heat exchangers is omitted, which is a common assumption in energy system analysis. This assumption is valid and does not significantly affect the outcomes.

The temperature and pressure of the PEMEC are assumed constant at 80 °C and 1 bar, which closely matches operational conditions, making this assumption logical [74]. Avoiding higher temperatures in PEMEC is due to design limitations and material constraints. This assumption facilitates comparison between different models and simplifies the analysis.

3. Governing equation

Energy, exergy, exergoeconomic, and exergoenvironmental (4E) analyses have been conducted on the proposed system. Furthermore, for optimization, the multi-objective dragonfly algorithm (MODA) has been utilized. These analyses were performed using MATLAB software. **Fig. 2** illustrates the flowchart of the proposed system analysis process, along with the application of optimization in the polygeneration system.

For the thermodynamic study of the proposed system, mass and energy balances have been employed. These balances are derived based on the first law of thermodynamics, enabling the examination of heat and power exchanged within the system. The equation corresponding to the mass and energy balance in a steady state condition is as follows [60]:

$$\dot{Q} - \dot{W} = \sum_{i=1}^{n} \dot{m}_{out} h_{out} - \sum_{i=1}^{n} \dot{m}_{in} h_{in} \tag{4}$$

$$\sum_{i=1}^{n} \dot{m}_{out} = \sum_{i=1}^{n} \dot{m}_{in} \tag{5}$$

In eq. 4, $\dot{Q}$ represents the rate of heat transfer, $\dot{W}$ denotes the rate of power generation, $\dot{m}_{in}$ and $\dot{m}_{out}$ are the mass flow rates entering and exiting the control volume, respectively. According to the principle of state convention, knowing two independent thermodynamic variables allows the calculation of other thermodynamic variables. For instance, knowing the temperature and pressure of the exiting flow from a turbine enables the calculation of its specific enthalpy. In this work, the specific enthalpy values are calculated using the REFPROP library in MATLAB, considering the fluid present in each stream.

Alongside mass and energy balances, some equipment requires additional auxiliary equations for a more comprehensive analysis. This is because the mass and energy equations consider the system in a closed state, examining only the input and output streams. To analyze mass transfer, heat transfer, or other important parameters, additional auxiliary equations must be considered for each equipment. Other equations used for the analysis of individual system components, along with known and unknown parameters, are presented in **Appendix Table A.1.**

In the current work, machine learning (ML) has been utilized to extract the governing relationships for the gasification process, ASU, and ammonia synthesis. The use of ML in modeling and simulating complex processes such as gasification and ammonia synthesis has significant advantages. One of the main advantages of using ML in this area is its ability to recognize complex patterns and nonlinear relationships in process data, enabling the creation of highly accurate process models that facilitate optimization and control.

Initially, simulations or modeling of these systems were performed in software, and then validation was carried out based on reputable references. For each of the systems, repetitive calculations were made to prepare input data, and using optimization algorithms such as genetic programming (GP), model parameters were automatically adjusted. Then, with the utilization of these optimized parameters and artificial intelligence network algorithms, governing relationships were accurately extracted. This algorithm (GP) manages a population of potential solutions and optimizes them through operations such as selection, mutation, and crossover to arrive at better and more optimal solutions. In the present work, GP has been employed to automatically adjust the model parameters, which is highly effective both in terms of time and accuracy and efficiency [77]. It is also worth mentioning that in this process, data weighting is determined using GP. Data weighting plays a crucial role in model training, as proper weighting of the data can improve the model's performance and prediction accuracy. **Fig. 3** illustrates the process of extracting relationships for energy systems using ML.

In the current study, Aspen Plus software has been employed for simulating the ASU, and the illuminating ML equations of Noorbakhsh et al. have been utilized. The extracted relationships are based on a combination of GP and KNN algorithms [78]. The simulation of the ammonia synthesis process in Aspen HYSYS software has been conducted based on reference [70], and a combination of GP and ANN has been utilized for extracting the governing equations. Additionally, the gasification process modeling has been performed using MATLAB

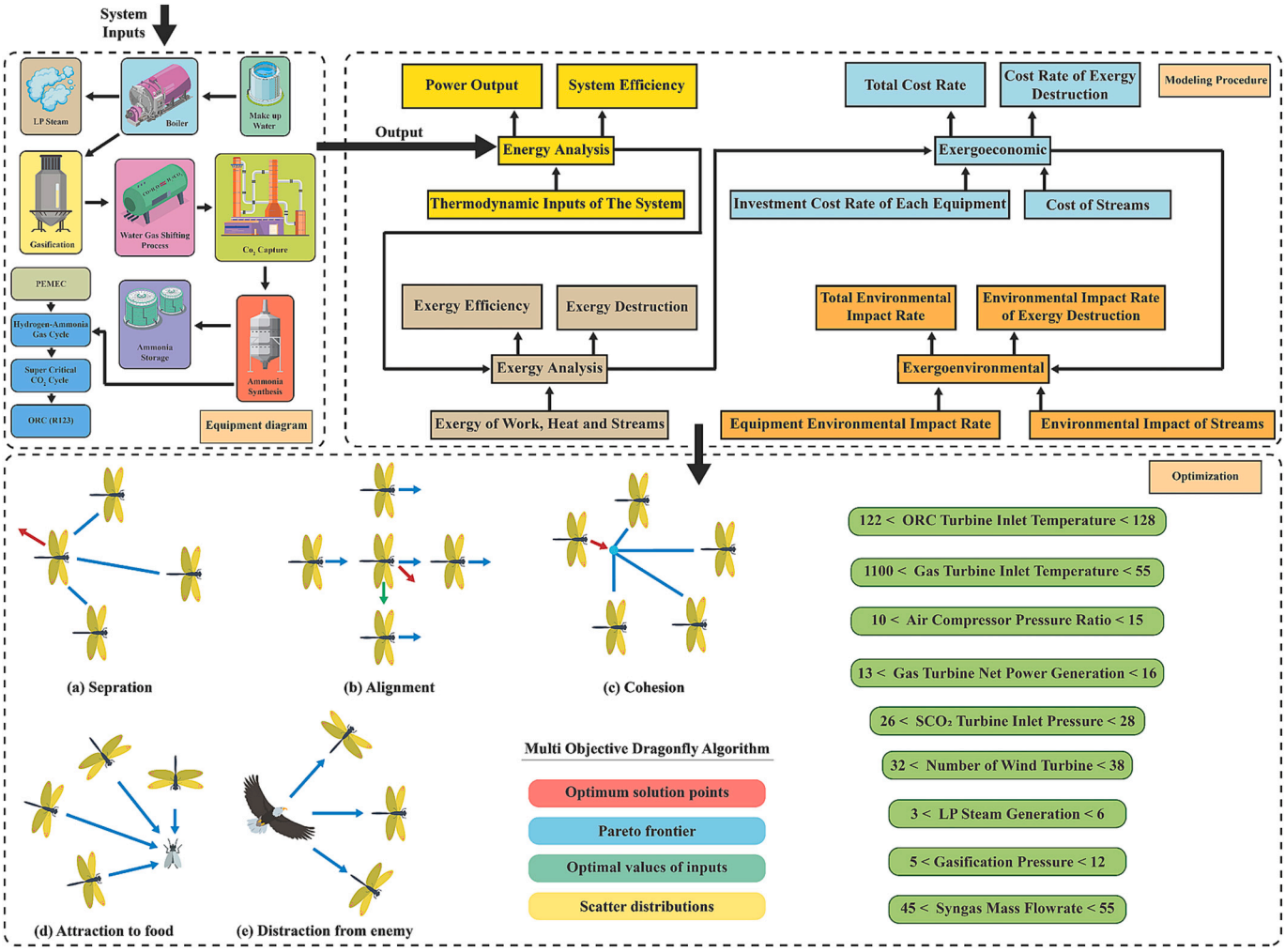

Fig. 2. Schematic of the analysis and optimization process of the proposed polygeneration system.

software, and its relationships have been extracted using a combination of GP and Deep ANN [57]. The relevant equations are provided in **Table A.1 in** the Appendix.

By analyzing exergy, derived from the second law of thermodynamics, it is possible to calculate the irreversibilities of an energy system. This analysis refers to the quality of energy, whereas energy analysis emphasizes energy quantity. Therefore, for a deep understanding of energy systems, this analysis is essential. Energy systems comprise three types of exergy: work exergy, heat exergy, and flow exergy. Eq. 6 represents the exergy balance [79].

$$\dot{E}x_Q + \sum_{i=1}^{n} \dot{m}ex_{in} = \sum_{i=1}^{n} \dot{m}ex_{out} + \dot{E}x_W + \dot{E}x_D \tag{6}$$

In which $\dot{E}x_Q$, $\dot{m}ex_{in}$, and $\dot{m}ex_{out}$ represent the exergy destruction, exergy inflow, and outflow, respectively. $\dot{E}x_Q$ and $\dot{E}x_W$ denote the exergy due to work production or consumption and the exergy due to heat transfer, respectively. The equations related to these two parameters are as follows [79].

$$\dot{E}x_W = \dot{W} \tag{7}$$

$$\dot{E}x_Q = \dot{Q}\left(1 - \frac{T_0}{T_s}\right) \tag{8}$$

Exergy of work is equal to the work done in the system. In eq. 8, $\dot{Q}$ represents the heat transfer rate, T_0 denotes the reference temperature, and T_s represents the actual temperature.

Exergy of work is defined for systems engaged in work exchange. Additionally, systems involved in heat transfer possess thermal exergy. Below, the relationship of solar and wind exergy is mentioned [72,80].

$$\dot{E}_{solar} = \dot{Q}_{solar}\left(1 - \frac{4}{3}\frac{T_a}{T_{sun}}(10 - 0.28lnf_{dil})\right) \tag{9}$$

$$\dot{E}_{Wind} = \frac{1}{2}\rho A V^3 \tag{10}$$

In Eq. 9, $\dot{Q}_{solar}$ represents solar heat, T_{sun} is the temperature of the sun, and T_a is the ambient temperature. Additionally, f_{dil} represents the dilution factor, with a value of 1.3×10^{-5} [81]. In Eq. 10, ρ denotes air density, A represents the swept area, and V denotes wind velocity [68].

Furthermore, flow exergy arises from the motion of the stream, comprising physical exergy and chemical exergy. Eq. 11 represents the physical exergy of each stream [79].

$$ex_{ph} = (h - h_0) - T_0(s - s_0) \tag{11}$$

h, h_0, s, and s_0 represent the specific enthalpy and entropy in actual and reference states, respectively.

Additionally, eqs. 12, 13, and 14 denote the chemical exergy of the mixture components (in the current work, these can refer to syngas, ammonia-hydrogen combustion gas), the chemical exergy of biomass, and the chemical exergy of hydrogen, respectively [82,83].

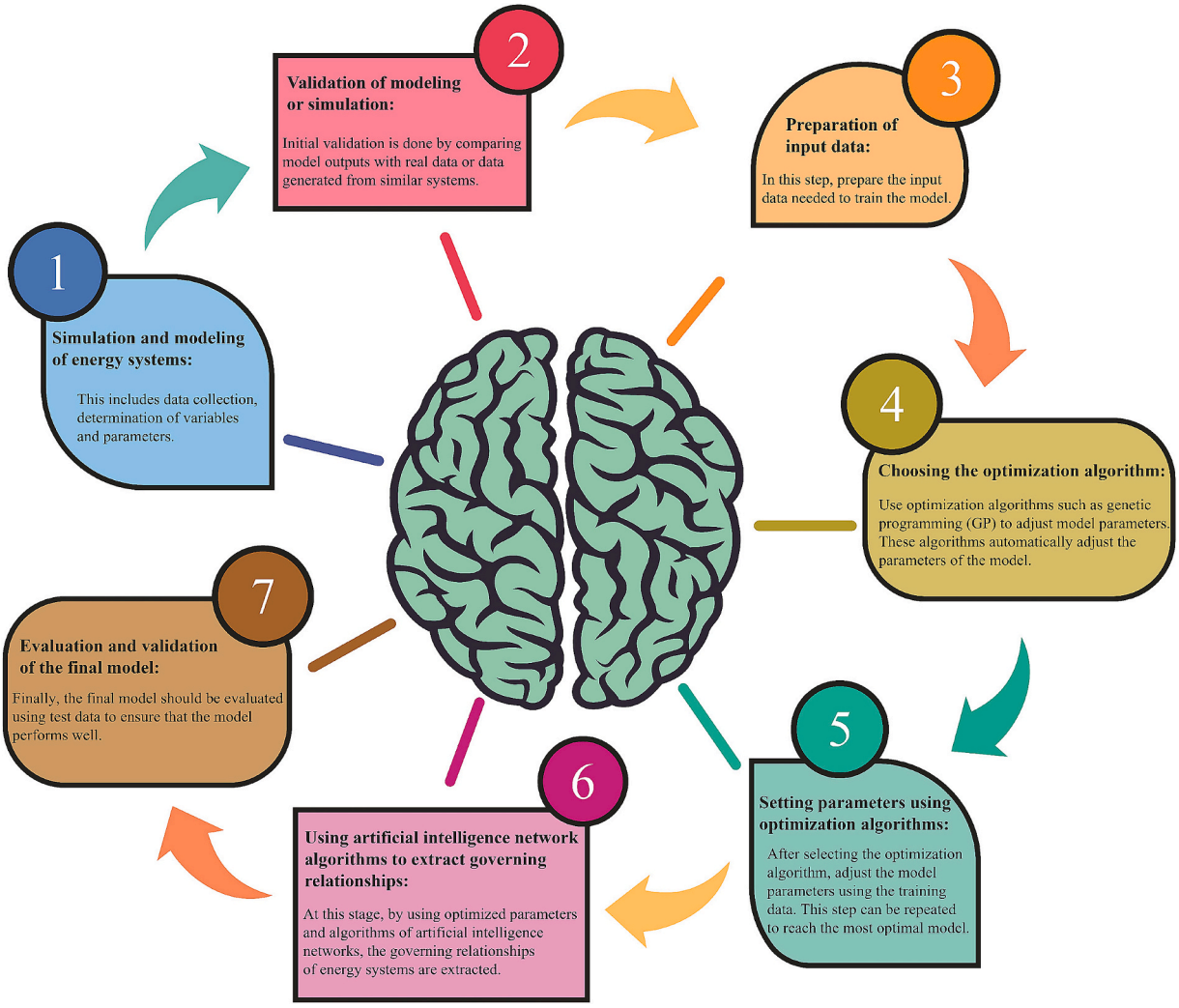

Fig. 3. The process of extracting the governing relationships of energy systems using ML.

$$ex_{ch}^{mix} = RT_0 \sum_{i=1}^{n} X_i ln X_i + \sum_{i=1}^{n} X_i ex^{ch_i} \tag{12}$$

$$ex_{ch}^{biomass} = \beta_{biomass} \times LHV_{biomass} \tag{13}$$

$$ex_{ch}^{hydrogen} = 0.985 \times LHV_{hydrogen} \tag{14}$$

Where T_0 is the reference temperature, R is the universal gas constant, X_i represents the mole fraction of the i-th component in the mixture, and ex^{ch_i} denotes the standard molar chemical exergy of the ith chemical species. $\beta_{biomass}$ can be calculated from eq. 15 [84].

$$\beta_{biomass} = \frac{1.0414 + 0.0177\left[\frac{H}{C}\right] - 0.3328\left[\frac{O}{C}\right]\left(1 + 0.0737\left[\frac{H}{C}\right]\right)}{1 - 0.4021\left[\frac{O}{C}\right]} \tag{15}$$

O, C, and H respectively represent the weight fractions of oxygen, carbon, and hydrogen.

The primary objective in exergy analysis is to determine the irreversibility of the system, or in other words, exergy destruction. Exergy destruction is a crucial metric for assessing the performance of energy systems, as it quantifies the amount of useful energy that is lost due to irreversibilities within the process. High levels of exergy destruction indicate inefficiencies that can be targeted for improvement.

Another method for determining exergy destruction is to analyze all components and equipment of the system separately and introduce the fuel exergy and product exergy for each component. This component-wise analysis allows for identifying specific areas where inefficiencies arise and enables focused optimization efforts. Eq. 16 expresses exergy destruction as a function of fuel exergy and product exergy [60].

$$\dot{E}x_D = \dot{E}x_F - \dot{E}x_P \tag{16}$$

Additionally, according to eq. 17, exergy efficiency is defined as the ratio of product exergy to fuel exergy [60].

$$\psi_{ex} = \frac{\dot{E}x_P}{\dot{E}x_F} \tag{17}$$

Exergy efficiency provides insight into how effectively the energy input is converted into useful work or products. A higher exergy efficiency signifies a more effective system with less exergy destruction, reflecting better performance and lower environmental impacts. By evaluating both exergy destruction and exergy efficiency, we can derive valuable insights into the system's operational effectiveness and guide future enhancements.

Exergoeconomic analysis has been conducted to examine the economic performance of the proposed system. This analysis provides the possibility of optimizing processes and systems based on economic costs, leading to reduced energy consumption, operational costs, and increased profitability in the system. Eq. 18 illustrates the exergoeconomic balance [60].

$$\sum_{i}^{N}\left(c_i\dot{E}x_i\right)_k+\dot{C}_Q+\dot{Z}_k=\sum_{e}^{N}\left(c_e\dot{E}x_e\right)_k+\dot{C}_W \tag{18}$$

In the above equation, $\dot{Z}_k$ and c represent the investment cost rate of each equipment and the cost stream per unit exergy, respectively. $\dot{Z}_k$ can be calculated from the following eq. [60].

$$\dot{Z}_k=\frac{PEC_k CRF\varphi}{3600N} \tag{19}$$

φ represents the maintenance factor, which in this work is considered as 10 %. CRF stands for the cost recovery factor, and its value is taken as 1.06. Moreover, N denotes the system's lifespan, assumed to be 20 years. The operating hours of the equipment during one year are assumed to be 3500 h for PTC, 6000 h for wind turbines, and 8000 h for other equipment [85]. Additionally, PEC refers to the equipment purchasing cost of the system. To calculate the value of PEC, one can directly obtain the equipment cost from the equipment manufacturer. Another method is to use equations developed based on thermodynamic parameters. These equations may not reach the accuracy of the first method, but they are suitable for a comprehensive feasibility study of the proposed system. The equations related to equipment costs are mentioned in **Table A.2** in the Appendix.

There are various methods for environmental analysis such as Life Cycle Assessment (LCA), water footprint, carbon footprint, and more. Among these analyses, the most comprehensive one is LCA. In this analysis, the emission of all environmental pollutants, including carbon dioxide, NO_x, SO_x, etc., is considered and expressed in points over the course of one year. This analysis evaluates the adverse environmental impacts of a product from production and transportation to disposal and burial and is based on Eco indicator 99, ISO 14040, and ISO 14044 standards [86]. Fig. 4 illustrates the stages of LCA.

Exergoenvironmental analysis has been conducted to examine the environmental impacts of the proposed system. The exergoenvironmental balance is provided below [85].

$$\sum_{i}^{N}\left(b_i\dot{E}x_i\right)_k+\dot{B}_Q+\dot{Y}_k=\sum_{e}^{N}\left(b_e\dot{E}x_e\right)_k+\dot{B}_W \tag{20}$$

In the above equation, $\dot{Y}_k$ and b represent the rate of environmental impacts of equipment and the environmental impacts of the stream per unit of exergy, respectively. $\dot{Y}_k$ can be calculated using the following eq. [85,87].

$$\dot{Y}_k=\frac{Weight_k\times b_{m,k}}{3600Nn} \tag{21}$$

In eq. 21, $Weight_k$ represents the weight of the equipment. Additionally, to obtain the weight of the equipment, two methods can be employed. The first method involves obtaining the precise weight from the manufacturer. The second method utilizes equations developed based on thermodynamic parameters to calculate equipment weight. The equations related to equipment weight are provided in **Table A.2** located in the Appendix. $b_{m,k}$ represents the environmental impacts, which are calculated per unit mass of the equipment using LCA analysis. The values related to the environmental impacts of the proposed system's equipment per unit mass can be observed in Table 4.

Furthermore, for the analysis and optimization of the proposed system, MATLAB software was utilized. Aspen HYSYS software was employed for simulating the ammonia synthesis unit, and Aspen Plus was utilized for simulating the ASU [78]. Python programming was used for implementing ML algorithms in sections related to ammonia synthesis, ASU, and gasification [57] (Fig. 5). The analyses performed on the proposed system are as follows:

- Energy analysis
- Exergy analysis
- Exergeoeconomic analysis
- Exergoenvironmental analysis
- Multi-objective optimization.

The results related to modeling and simulation are provided below.

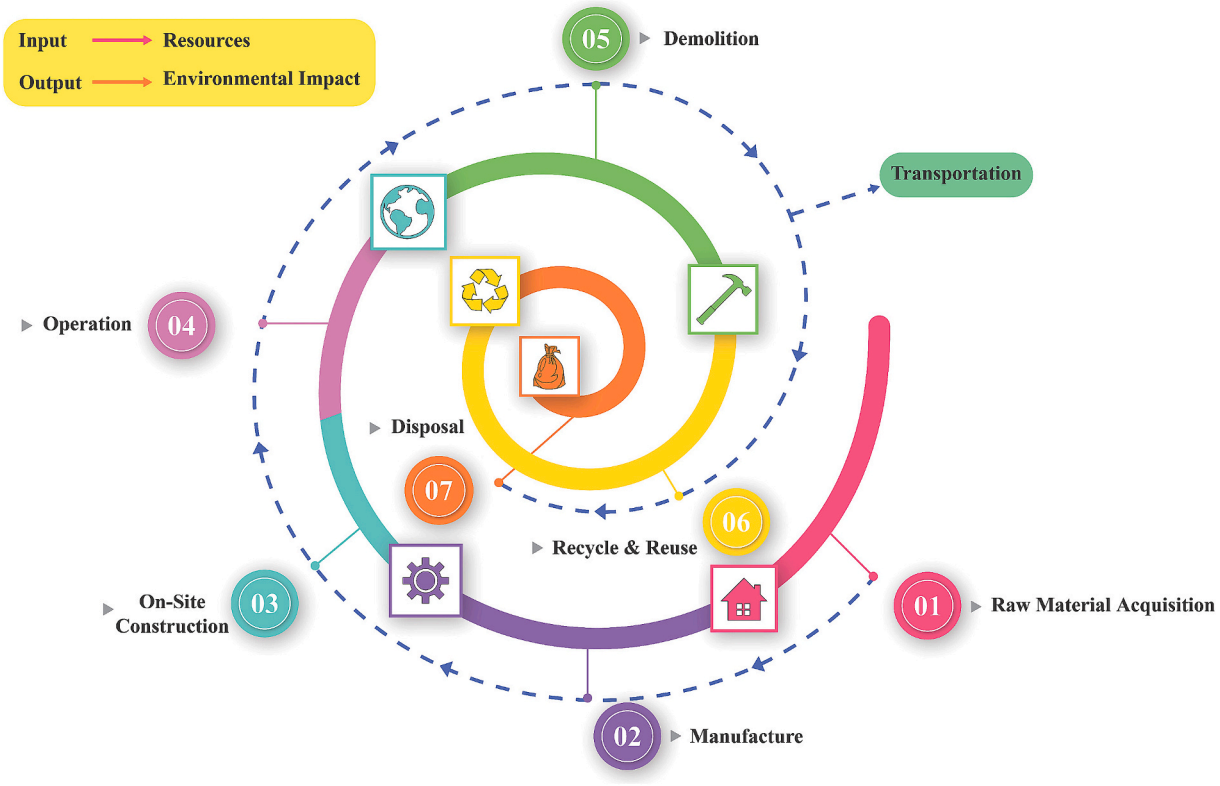

Fig. 4. LCA steps from extraction of raw materials to disposal.

Table 4
Environmental impacts of each equipment in presented system [49,83,85].

Component	Material Composition	Eco' 99 Indicator (mPts/kg)	Material (mPts/kg)	Process (mPts/kg)	Disposal (mPts/kg)	Total (mPts/kg)
Compressors	Steel 33,33 %	86	130	11.7	−70.0	71.7
	Steel low alloy 44,5 %	110				
	Cast iron 22,22 %	240				
Combustion Chamber	Steel 33,34 %	86	635	20.0	−70.0	585
	Steel high alloy 66.66 %	910				
Turbines	Steel 25 %	86	704	12.1	−70.0	646
	Steel high alloy 75 %	910				
Pumps	Steel 35 %	86	186	16.9	−70.0	132.8
	Cast iron 65 %	240				
Gasifier	Steel 100 %	86	86	12.1	−70.0	28.0
Feed water	Steel 100 %	86	86	12.1	−70.0	28.0
Heat Exchangers	Steel 100 %	86	86	12.1	−70.0	28.0
Wind Turbine	Aluminum 80 %	780	841.2	8.8	−70.0	780
	Steel 20 %	86				
Collectors	Steel 98 %	86	85	7.3	−69.0	23.2
	Glass 2 %	58				
Columns	Steel 100 %	86	86	12.1	−70.0	28.0
PEMEC	Steel low alloy 34 %	110	–	–	–	111.58
	Steel high alloy 13 %	910				
	Concrete 40 %	3.8				
	Electronic material 8 %	–				
	Plastic 2 %	330				
	Copper 1 %	1400				
	Aluminum 1 %	780				
	Process Material 1 %	–				
Reactors	Steel 100 %	86	86	12.1	−70.0	28.0
Boiler	Steel 25 %	704	12.1	−70.0	704	646
	Steel high alloy 75 %					

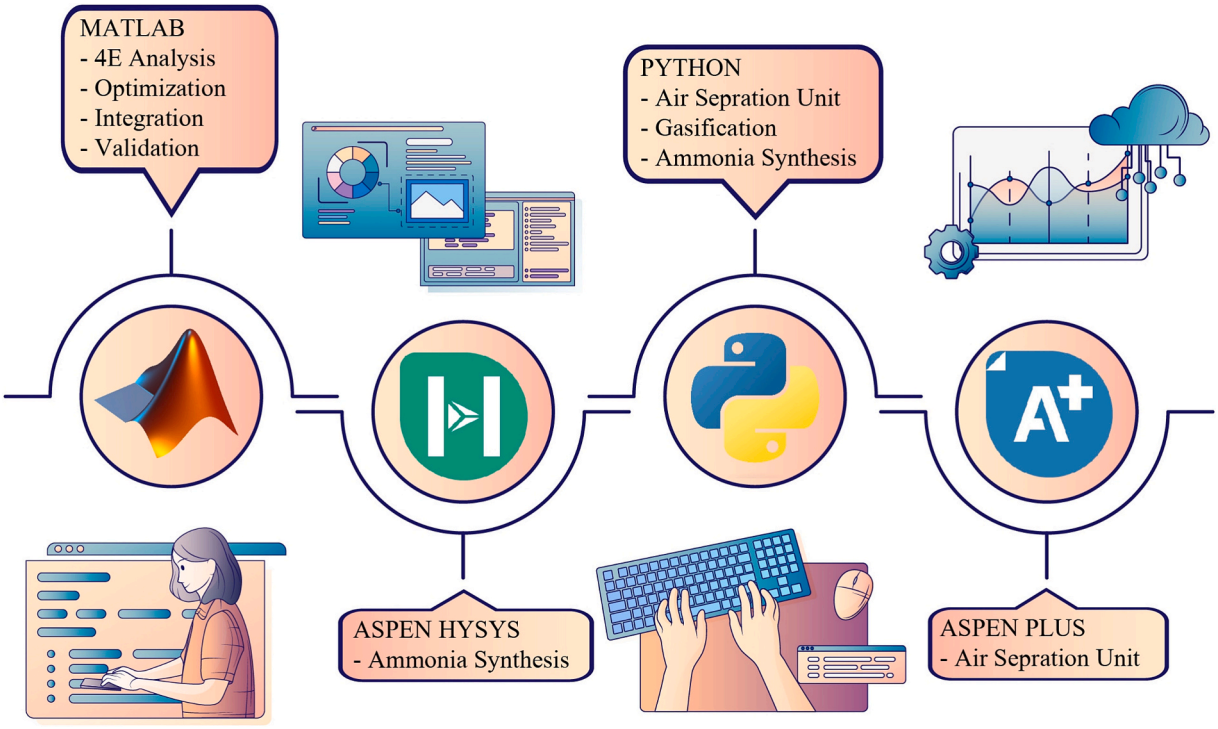

Fig. 5. The use of different software to check and analyze the presented polygeneration system.

4. Results

4.1. Modeling validations

The thermodynamic validation of the proposed system, which includes sections such as the hydrogen-ammonia gas cycle, S-CO_2 cycle, ORC, ammonia synthesis, PEMEC, PTC, wind turbine, and gasification, has been conducted based on reputable articles. The validation of the PEM electrolyzer (PEMEC) has been conducted based on previously published work [83], and the results demonstrate a strong agreement with experimental data. Similarly, the ammonia synthesis unit has been simulated using Aspen HYSYS and validated against data from [70], with an average validation error below 5 %. The gasification process validation is also based on the study conducted by Mousavi Rabeti et al. [30], showing minimal differences compared to experimental results. These validations confirm the reliability of the models used in this study. The validation of PTC in the study [83], conducted by the authors of this research, has been previously demonstrated. Furthermore, modeling of the S-CO_2 cycle, ORC, and hydrogen-ammonia gas cycle was performed using MATLAB software, and then the results were compared and validated with the articles [15,75,76]. The validation results of this section can be observed in Table 5 and Table 6. The validations conducted have been compared with the referenced articles, and their results show the least error. Therefore, it can be stated that the validations have been performed correctly and acceptably. The wind turbine modeling has been carried out in MATLAB software, and the wind turbine model used is LTW77 [72]. The model validation has been conducted using the power curve provided by the manufacturer. Fig. 6 illustrates the results of this validation, indicating its credibility.

Table 6
Validation results of different parameters for S-CO_2 cycle, ORC and hydrogen-ammonia gas cycle.

Parameters	Section	Ref.	Code	Error
Net power output (MW)	ORC (R123) [76]	43.8	43.05	1.70
Total thermal efficiency		0.153	0.151	1.04
Net power generation (MW)		2.18	2.228	2.20
Heat transfer in recuperator (MW)	S-CO_2 cycle [75]	6.13	6.146	0.26
Heat transfer in precooler (MW)		5.06	5.062	0.04
Air compressor power input (MW)		12.897	12.71	0.14
Gas turbine power output (MW)	Hydrogen-ammonia gas cycle [15]	2.98	2.79	6.00
Net power output (MW)		9.917	9.917	0.00

4.2. 4E analysis

Energy, exergy, exergoeconomic, and exergoenvironmental analyses have been employed to investigate the proposed system. Table 7 presents the results of these analyses for each equipment of the system. It is observed that the highest exergy destruction rates in the considered system are attributed, respectively, to the ASU, gasifier, and ammonia production unit (APU). In addition, the detailed thermodynamic stream characteristics of the proposed system have been summarized in **Table A.3** in the Appendix for further reference. In the ASU, the deep cooling process with high energy consumption can lead to increased irreversibility and consequently, an increase in exergy destruction, cost destruction, and environmental impact deterioration in this system. Following the ASU, the majority of exergy destruction is associated with

Table 5
Validation results of S-CO_2 cycle, ORC and hydrogen-ammonia gas cycle.

No.	Type	T_{Ref}	T_{code}	Error	P_{Ref}	P_{code}	Error	$\dot{m}_{Ref}$	$\dot{m}_{code}$	Error
					ORC (R123) [76]					
1	R123	40.00	40.04	0.11	1.55	1.55	0.00	1.45	1.44	0.84
2	R123	40.23	40.25	0.04	5.81	5.81	0.00	1.45	1.44	0.84
3	R123	53.02	55.42	4.52	5.81	5.81	0.00	1.45	1.44	0.84
4	R123	86.94	87.01	0.08	5.81	5.81	0.00	1.78	1.81	1.28
5	R123	87.39	87.45	0.06	12.01	12.01	0.00	1.78	1.81	1.28
6	R123	120.00	123.00	2.50	12.01	12.01	0.00	1.78	1.81	1.28
7	R123	95.96	98.73	2.89	5.81	5.81	0.00	0.33	0.36	9.12
8	R123	62.91	65.42	3.99	5.81	5.81	0.00	1.45	1.44	0.84
9	R123	44.77	43.77	2.22	1.55	1.55	0.00	1.45	1.44	0.84
					S-CO_2 cycle [75]					
1	CO_2	378.90	378.90	0.00	273.20	273.20	0.00	29.00	29.04	0.14
2	CO_2	260.00	260.05	0.02	88.00	88.04	0.00	29.00	29.04	0.14
3	CO_2	86.39	86.19	0.23	87.60	87.62	0.00	29.00	29.04	0.14
4	CO_2	36.85	36.85	0.00	87.20	87.20	0.00	29.00	29.04	0.14
5	CO_2	79.36	79.27	0.11	276.00	276.00	0.00	29.00	29.04	0.14
6	CO_2	191.95	192.08	0.07	274.60	274.60	0.00	29.00	29.04	0.14
					Hydrogen-ammonia gas cycle [15]					
1	Air	25	25	0.00	1.01	1.01	0.00	7.90	7.95	0.63
2	Air	367.00	392.00	6.81	13.00	13.17	1.31	7.90	7.95	0.63
3	Exhaust gas	1291.00	1291.00	0.00	13.00	13.17	1.31	9.14	9.19	0.55
4	Exhaust gas	693.90	676.10	2.56	1.01	1.01	0.00	9.14	9.19	0.55
5	Ammonia	−33.00	−33.00	0	1.01	1.01	0.00	1.22	1.23	0.82
6	Hydrogen	100.00	100.00	0	1.01	1.01	0.00	0.014	0.014	0.00

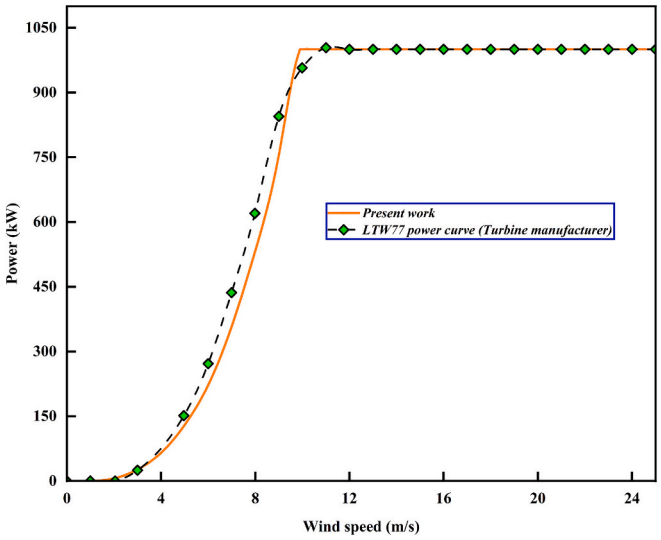

Fig. 6. Validation of the present working wind turbine with the manufacturer's power curve.

the APU and gasifier units. In these units, various chemical reactors exist, which may lead to an increase in entropy and consequently exergy destruction. Moreover, from the definition of exergy destruction, it is evident that the ratio of fuel exergy to product exergy in these systems is higher than in other equipment, leading to a decrease in exergy efficiency. Therefore, improving the performance of the proposed system through optimizing the ASU is highlighted as the most crucial aspect. Additionally, although exergy destruction in the gasifier and APU is significant, considering their higher exergy efficiency compared to some other equipment, they are not prioritized for improvement. PTC and OFOH are the next priorities for performance enhancement, and operational conditions and materials of these units should be improved in the design phase.

In the proposed system, the highest capital investment cost is attributed to the solar and wind sections of the system. Although the use of renewable energies has led to a reduction in environmental impacts in the proposed system, it has also had a significant impact on the capital investment costs. Among the reasons for this, the materials used in these equipments can be mentioned, which is expected to improve with technological advancements in the field of renewable energies in the future years, leading to a reduction in capital investment costs. The highest cost destruction is related to the ASU, Boiler, and APU. In these equipments, exergy destruction and fuel costs per exergy unit are high, resulting in increased cost destruction.

The highest environmental impacts in the system are attributed to the S-CO_2 turbine (S-CO_2T) equipment, primarily due to its high weight. Another reason is that the significant pressure drop in turbines leads to environmental effects. Following that, ASU and expander have the highest environmental impacts, which is also justifiable for similar reasons. The greatest environmental impact destruction is related to ASU, APU, and gasifier, which are justifiable for similar reasons as well. Additionally, it should be noted that due to diverse chemical reactions in the combustion chamber (CC) and the high environmental effects of fuel per exergy unit, the environmental impacts of this equipment are also considerable.

Fig. 7 illustrates the exergy destruction, cost destruction, and environmental impact destruction diagrams of the system. As previously explained, the ASU is more destructive in terms of exergy destruction, cost destruction, and environmental impact destruction compared to other sections. Additionally, due to high energy consumption and significant losses, the APU exhibits considerable exergy destruction after the ASU. It is necessary to recover these losses in the system to reduce exergy destruction. The use of solar energy for the boiler reduces environmental impacts for this equipment but increases the cost destruction. In the ammonia-hydrogen gas cycle, significant exergy destruction, cost

Table 7
Results of analyses all component used in the proposed polygeneration system.

Component	*Exergy analysis*		*Exergoeconomic analysis*		*Exergoenvironmental analysis*	
	$\epsilon_k(\%)$	$\dot{E}x_{D_k}(MW)$	$\dot{Z}_k(\$/hr)$	$\dot{C}_{D_k}(\$/hr)$	$\dot{Y}_k(mPts/hr)$	$\dot{B}_{D_k}(mPts/hr)$
Boiler	44.98	17.41	60.08	1027.74	40.13	2530.07
P1	80.00	0.00	0.01	0.00	0.02	0.64
P2	85.34	0.00	0.01	0.00	0.00	0.54
P3	85.34	0.00	0.01	0.00	0.00	0.72
SHX1	76.88	0.98	3.91	111.14	2.00	55.42
SHX2	81.46	1.91	7.33	218.01	3.59	108.71
PTC1	33.97	8.23	480.67	0.00	239.68	0.00
PTC2	33.80	20.19	1175.94	0.00	586.38	0.00
Gasifier	61.55	122.02	26.93	566.94	152.43	14,195.39
Expander	95.32	0.50	7.87	3.87	8524.85	95.59
APU	70.64	108.70	116.16	1066.75	51.50	21,955.95
WT	44.00	15.60	785.75	0.00	1.03	0.00
ASU	33.02	222.22	236.77	14,249.29	9654.68	175,082.06
PEMEC	65.33	1.21	54.45	77.69	35.62	954.55
AC	95.27	0.21	22.65	20.14	14.31	418.47
CC	47.17	26.00	2.39	719.48	914.48	12,619.68
AGT	74.31	4.07	205.44	239.40	6690.15	4352.21
SCO_2Hx	73.30	1.33	3.09	78.07	1.60	1419.33
SCO_2 T	94.09	0.22	8.94	25.81	21,963.69	1017.06
Rec	81.16	0.40	2.71	47.53	1.42	1872.79
SCO_2 C	87.27	0.13	1.83	17.16	63.08	1507.40
Pre-cooler	–	1.05	2.35	–	1.24	–
ORC Eva	67.02	0.16	0.83	9.60	0.47	174.56
ORCT	75.36	0.08	1.64	156.00	1110.99	2155.65
HE	76.58	0.00	0.12	5.00	0.08	69.09
ORCP1	94.80	0.00	0.01	0.03	0.01	1.08
OFOH	18.84	0.26	10.91	622.48	2.10	8610.76
ORCP2	79.33	0.00	0.02	0.22	0.03	8.58
Geo Hx	87.82	0.00	0.14	0.02	0.09	0.00
ACC	–	0.38	0.05	–	0.02	–

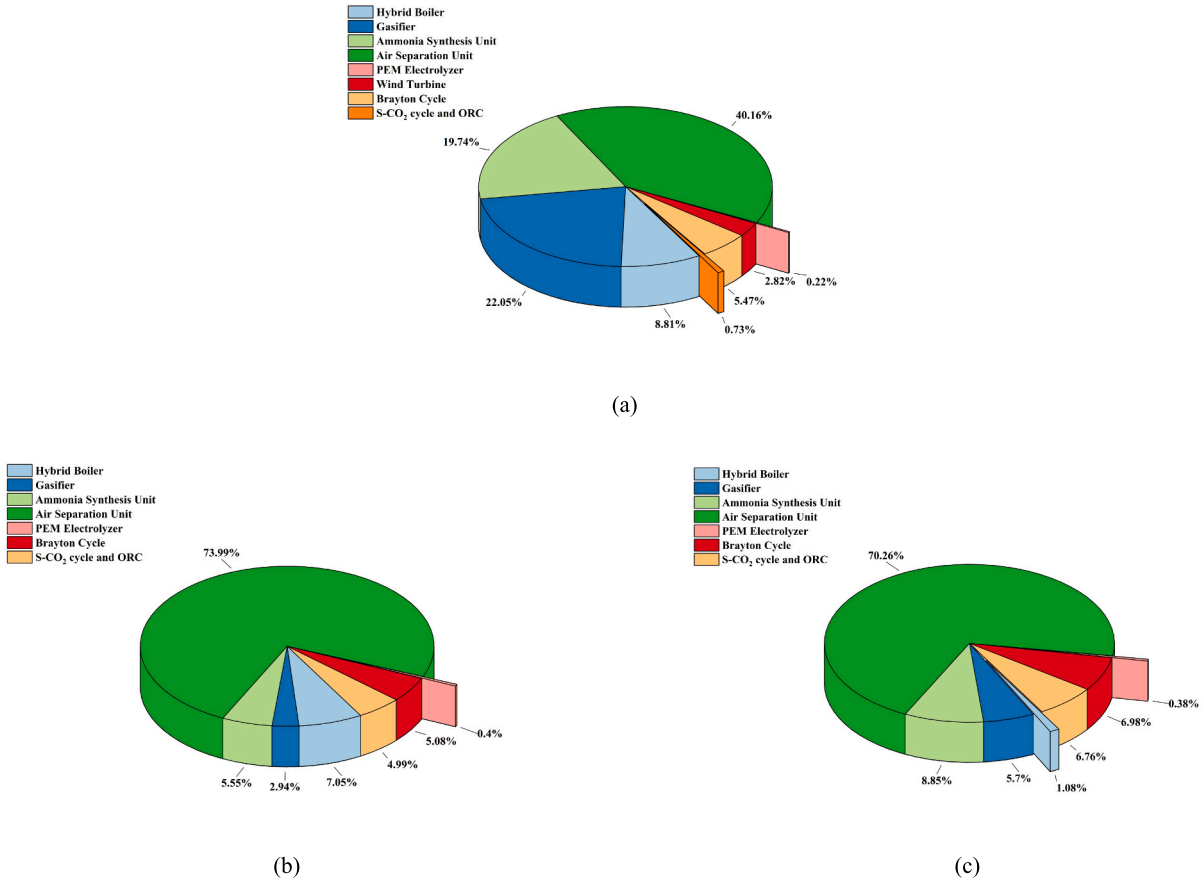

Fig. 7. (a) Exergy Destruction, (b) cost destruction, and (c) environmental impact destruction contributions of all parts in the proposed polygeneration system.

Table 8
Overall result of 4E analysis of the proposed system.

Parameters	Value
Net power generation (MW)	17.93
Net ammonia flow rate production (ton/day)	297.86
Mass flow rate of LP steam generation (kg/s)	5
Mass flow rate of oxygen generation (ton/day)	52.30
Overall polygeneration energy efficiency (%)	31.33
Total exergy destruction (MW)	553.31
Overall polygeneration exergy efficiency (%)	38.53
Total cost rate of polygeneration system ($/h)	5631.22
Total environmental impact rate of polygeneration system (Pts/h)	53.16
Levelized cost of electricity ($/MWh)	0.05
Levelized cost of ammonia production ($/kg)	0.06
Net present value (Million USD)	682.41
Internal Rate of Return (IRR) of the system (%)	30
Levelized environmental impact of electricity (mPts/kWh)	2.79
Levelized environmental impact of ammonia production (mPts/kg)	1.55
MSW mass flow rate consumption (kg/s)	9.38
Geothermal mass flow rate consumption (kg/s)	1.67
Number of wind turbines (model: LTW77)	35
Area of PTC (model: ET-100) in the solar field (Hectares)	13.12

destruction, and environmental impacts are observed. The reason for this, as mentioned earlier, is the presence of chemical reactions and the release of a considerable amount of energy in the CC, which needs improvement. Wind turbines exhibit considerable exergy destruction, but their cost destruction and environmental impact destruction are zero. This indicates that wind farms can be very effective in reducing costs and environmental impacts.

Table 8 presents the overall results of the analyses conducted on the proposed system. As evident, the values for Net power generation, Total exergy destruction, overall polygeneration exergy efficiency, total cost rate of the polygeneration system, net present value, and total environmental impact rate of the polygeneration system are 17.93 MW, 553.31 MW, 38.53 %, 5631.22 $/h, 682.41 Million USD, and 53.16 Pts/kWh, respectively.

The proposed polygeneration system comprises three main products: ammonia, power, and heat (process steam). In this study, the current work has been compared with other similar studies in terms of performance, and Table 9 illustrates this comparison. The study by Shamsi et al. exhibits the highest production rate of ammonia, with a value of 2.085 kg/s compared to other presented works. They were also able to generate 62.57 MW of power, which is approximately three times the power generated in the present study. Although their system generates more power due to the ORC and APU subsystems, the current work has more subsystems that consume additional power, indicating satisfactory performance given the higher production rates of other products in the current study. Additionally, the payback period in this study is comparable to that of Shamsi et al., at around 3 years, indicating a more economically viable performance of the proposed system considering the number of equipment used. The proposed system incorporates ammonia storage, which enhances system reliability and stability by effectively managing energy availability. Through ammonia production and storage, the system can convert renewable energy into storable chemical energy, ensuring continuous energy supply even during periods of low renewable energy generation. This feature significantly improves the system's ability to handle fluctuations inherent in renewable sources like solar and wind, thereby providing a reliable and stable energy output. Furthermore, the stored ammonia can be used to produce power or serve as an energy backup, thus preventing interruptions in system performance and enhancing overall efficiency. From an environmental perspective, the proposed system in the current study also utilizes a combination of three renewable energies, providing a more

Table 9
Comparison of the proposed system with similar systems.

Authors	Year	Energy sources	Products	Energy efficiency (%)	Exergy efficiency (%)	Ammonia	Heating	Total power
Present study	2024	Wind Solar Biomass Geothermal	Ammonia Power Heating	31.33	38.53	3.45 kg/s	14.06 MW	17.93 MW
Shamsi et al. [88].	2024	Geothermal	Ammonia Power Hydrogen Oxygen Hot water Cold water	10.71	50	2.085 kg/s	18.38 MW	62.57 MW
Hajimohammadi Tabriz et al. [50].	2023	Biomass Urban sewage	Heating Power Hydrogen Freshwater	35.48	40.18	–	47.440 MW	17.75 MW
Xing et al. [89].	2022	Geothermal Biomass	Heating Power Hydrogen Cooling	79.47	17.87	–	34.13 MW	22.23 MW
Xu et al. [90].	2021	Biomass	Ammonia Power	50.95	51.50	1.10 kg/s	–	20.71 MW
Tukenmez et al. [18].	2021	Solar Biomass	Ammonia Power Hydrogen Heating	58.76	55.64	0.33 kg/s	–	20 MW
Ansari et al. [91].	2021	Geothermal	Power Hydrogen Cooling Freshwater	49.1	67.9	–	4.26 MW	22.1 MW
Demir and Dincer [92]	2021	Solar	Ammonia Power Freshwater	70.3	12.1	0.85 kg/s	–	17.6 MW
Luqman et al. [93].	2020	Solar Wind	Power Freshwater Hydrogen Oxygen Cooling Water heating Hot air	50	34	–	–	11.40 MW

suitable basis for environmental preservation. Furthermore, it is observed that in the study by Tukenmez et al., by presenting a system based on solar and biomass energy, they were able to produce 20 MW of power. In comparison, the proposed system in the current study has a heating product with a production of 14.06 MW. However, it is noted that the ammonia production rate in the present work outperforms all reported researches. By comparing the present work with the research conducted by Demir et al., it becomes evident that they have a higher energy efficiency. However, the reason for this difference lies in the utilization of various and multiple subsystems in the current study. Additionally, the incorporation of wind and geothermal energy along with solar energy significantly impacts energy efficiency. Furthermore, in the present study, the proposed system also exhibits better performance in other comparable parameters. Overall, it is evident that the system presented in the production section, especially in the production of ammonia, exhibits the best performance compared to similar systems. These results demonstrate that the proposed polygeneration system not only achieves high ammonia production but also maintains competitive energy and exergy efficiencies, confirming its viability compared to existing systems. Additionally, despite the utilization of various and multiple subsystems and the incorporation of three renewable energies (wind, solar, and geothermal) in the present study, it demonstrates satisfactory performance both economically and environmentally. It has appropriate energy and exergy efficiencies and is justified compared to other studies. The proposed system is particularly well-suited for industrial and regional applications in areas rich in renewable energy resources. Specifically designed for Tehran, it capitalizes on the city's abundant solar, wind, and biomass potential, while also utilizing significant MSW generated in the region. Compared to similar systems (as highlighted in Table 9), this design offers superior energy efficiency, reduced environmental impact, and lower operational costs, making it ideal for real-world applications such as sustainable ammonia production in industrial zones and clean energy solutions for urban power grids. The system's flexibility and scalability further enhance its practicality, enabling its deployment across diverse industrial and urban scenarios, particularly in regions transitioning to renewable and sustainable energy solutions.

4.3. Sensitivity analysis

Sensitivity analysis in polygeneration systems allows for the identification of the effects of parameter variations on system performance, leading to a better understanding of system performance. This analysis enables the identification of parameters that have the greatest impact on system performance and facilitates necessary optimizations on these parameters. In this study, contour plots have been utilized for sensitivity analysis.

In Fig. 8**a**, variations in polygeneration efficiency concerning changes in two parameters, TIT Turbine Inlet Temperature (TIT) and gasification pressure, are illustrated. It is evident that with an increase in TIT, the polygeneration efficiency rises. The reason behind this is that as the temperature increases, although fuel consumption rises, it also leads

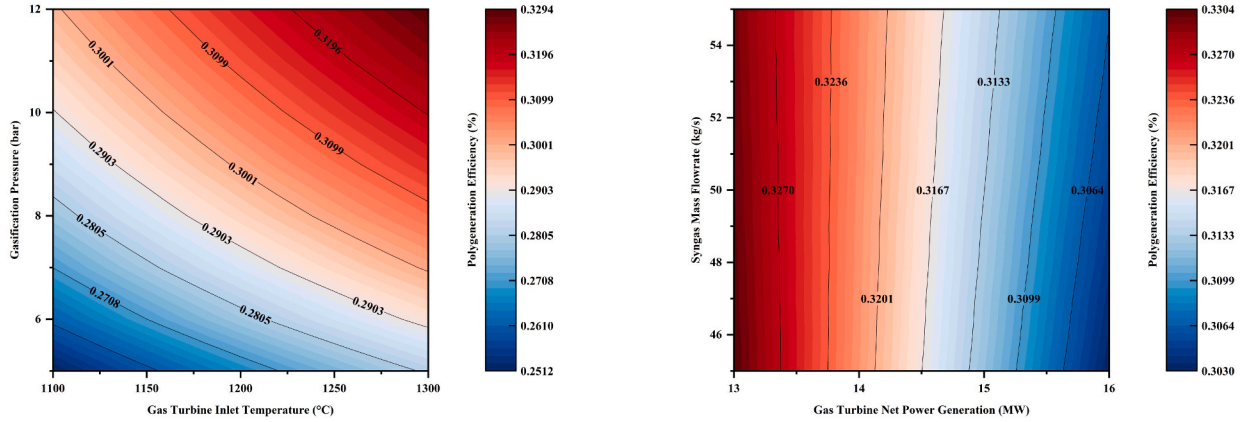

(a) (b)

Fig. 8. Investigating the changes of two parameters (a) TIT and gasification pressure as well as two parameters (b) gas turbine net power generation and syngas mass flow rate on total polygeneration efficiency

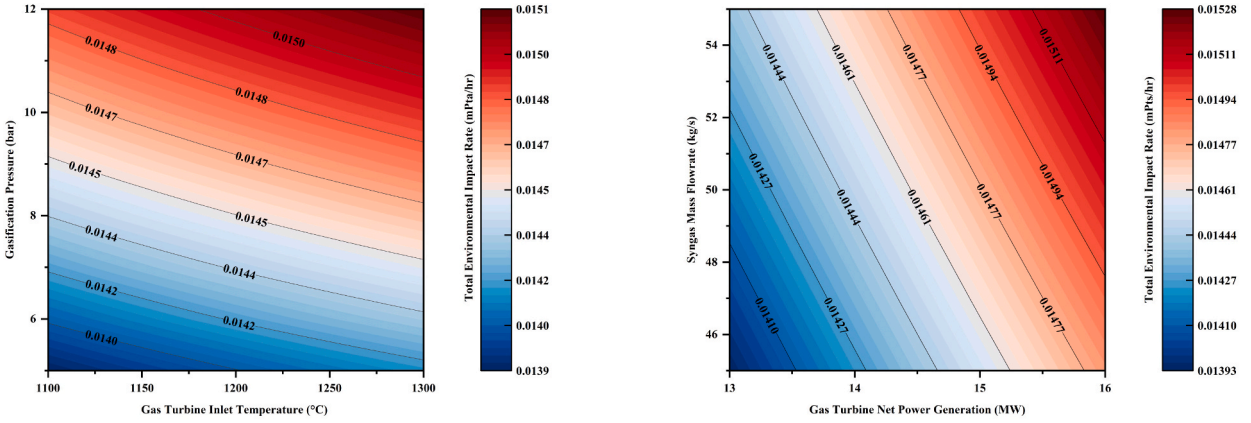

(a) (b)

Fig. 9. Investigating the changes of two parameters (a) TIT and gasification pressure as well as two parameters (b) gas turbine net power generation and syngas mass flow rate on total environmental impact rate

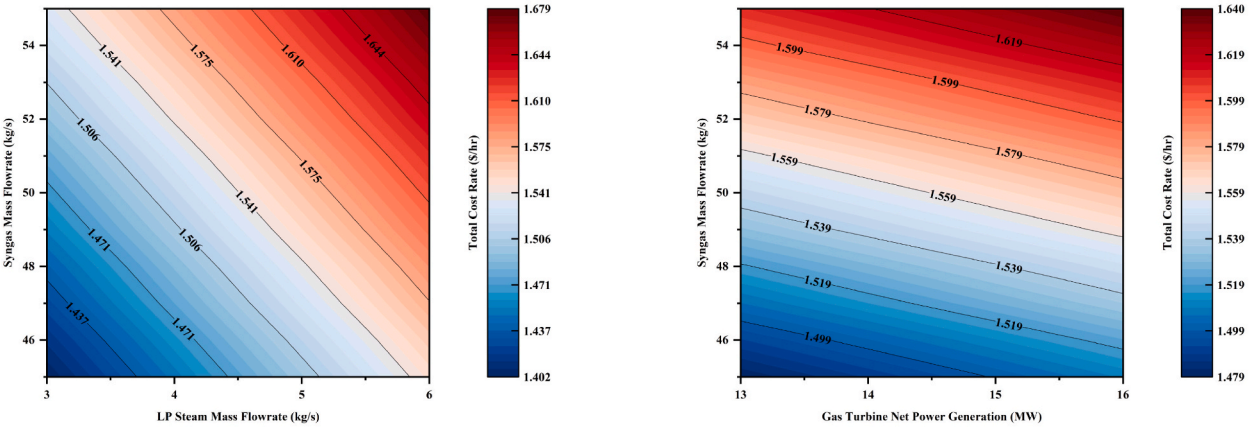

(a) (b)

Fig. 10. Investigating the changes of two parameters (a) LP steam mass flow rate and syngas mass flow rate as well as two parameters (b) gas turbine net power generation and syngas mass flow rate on total cost rate

to an increase in temperature and flue gas flow rate. This increase in temperature and flow rate can enhance power generation in lower-level cycles such as ORC and S-CO_2 cycles. Additionally, increasing the gasification pressure elevates the pressure in syngas, reducing pressure drop in power generation and ammonia synthesis stages, which results in increased efficiency of the polygeneration system.

Changes in polygeneration efficiency based on variations in two parameters, gas turbine net power generation, and syngas mass flow rate, are depicted in Fig. 8**b**. As evident, with an increase in gas turbine net power generation, the system efficiency decreases, which could be attributed to the increased fuel consumption. Additionally, it can be observed that with an increase in syngas mass flow rate, the system efficiency remains almost constant with very minimal changes. The reason for this is that as the flow rate increases, the power generation in the expander also increases. However, simultaneously, the amount of produced ammonia, which is the fuel for the gas cycle, also increases. This process results in negligible overall changes in polygeneration efficiency.

By examining Fig. 9**a**, it becomes apparent that as the TIT increases, the fuel consumption also increases, leading to higher environmental impacts. Furthermore, the increased fuel consumption results in a higher volume of flue gas, which could potentially increase the weight of equipment used in the lower-tier cycles and have significant environmental impacts. Additionally, with an increase in gasification pressure, the consumption of biomass increases, and the volume and weight of the gasifier also increase, contributing to higher environmental impacts. Therefore, to minimize environmental impacts, both TIT and gasification pressure should be kept as low as possible.

Based on Fig. 9**b**, it is evident that reducing the gas turbine net power generation results in a decrease in the weight of equipment used in the lower tier cycles due to reduced fuel consumption. This leads to a reduction in environmental impacts. Additionally, reducing the syngas mass flow rate decreases the consumption of biomass in the system, resulting in less equipment weight needed for gas synthesis, further reducing environmental impacts.

Based on Fig. 10**a**, it is evident that with an increase in both the syngas mass flow rate and the LP steam mass flow rate, the total cost rate of the system increases. This is because of the higher consumption of biomass for steam and syngas production.

As evident from Fig. 10**b**, the lower the gas turbine net power generation, the lesser the need for equipment with smaller dimensions and lower weights, thus reducing system costs, although the changes are not significant. Furthermore, as previously mentioned, higher syngas mass flow rate leads to increased biomass consumption in the system, resulting in an increase in the total cost rate. To minimize costs, it is advisable to have lower power generation, which, based on previous analyses, also leads to better efficiency in the system.

4.4. Optimization

Optimization of three- and four-objective functions has been performed using the dragonfly algorithm on the proposed system. The decision variables are presented after sensitivity analysis according to Table 10. Additionally, the objective functions for optimization are observable in Table 11.

Table 11
Objective functions considered for multi-objective optimization of the proposed system.

No.	Symbols	Description	Unit
$F_1(x)$	η_{Poly}	Polygeneration Efficiency	%
$F_2(x)$	$\dot{E}x_{D_{tot}}$	Total Exergy Destruction	MW
$F_3(x)$	$\dot{C}_{tot}$	Total Cost Rate	$/h
$F_4(x)$	$\dot{B}_{tot}$	Total Environmental Impact Rate	Pts/h

MODA has evolved based on the collective behavior of dragonflies in nature. One interesting feature about dragonflies is their unique group behavior. Dragonflies gather in groups for only two reasons: hunting and migration. The former is referred to as static (feeding) grouping, and the latter as dynamic (migration) grouping. In static grouping, dragonflies form small groups to fly to hunt other insects. Local movements and sudden changes in flight paths are key features of a static group. However, in dynamic grouping, a large number of dragonflies gather to migrate in one direction for long distances.

The main motivation behind the dragonflies algorithm stems from the behaviors of static and dynamic groups. These two group behaviors closely resemble the two primary phases of optimization using metaheuristics, namely exploration and exploitation. In the static grouping, dragonflies create subgroups and fly over different areas, which is primarily aimed at the exploration phase. However, in the dynamic grouping, dragonflies fly in larger groups and in one direction, which serves the objectives of the exploitation phase [94]. The collective behavior of dragonflies follows three fundamental principles: separation, alignment, and cohesion. The primary goal of each group (static and dynamic) is survival, so dragonfly behavior includes foraging for food sources and avoiding external threats. Taking these two behaviors into account, five main factors contribute to the formation of the

Table 12
Four-objective and three-objective optimization results of the proposed system.

Type of parameters	Symbol	Base case	Four objective optimization	Three objective optimization
Decision Variables	P_{GF}	9	7.95	8.65
	$\dot{m}_{sg}$	50	45.13	45.11
	TIT_{GT}	1291	1190.40	1264.86
	$\dot{W}_{net_{GT}}$	15	13.00	13.00
	$\dot{m}_{LP_{steam}}$	5	5.11	3.17
	n_{WT}	35	32	32
	$r_{P_{AC}}$	13	11.86	15.00
	TIP_{SCO2T}	27.32	28.00	27.56
	TIT_{ORCT}	123	126.83	127.82
Objective Functions	η_{Poly} (%)	31.33	30.88	31.69
	$\dot{E}x_{D_{tot}}$(MW)	553.31	525.19	**
	$\dot{C}_{tot}$ ($/hr)	5631.22	4989.97	4867.92
	$\dot{B}_{tot}$ (mPts/hr)	53.16	48.97	49.01

Table 10
Selected decision variables for multi-objective optimization of the proposed system.

NO.	Symbols	Description	Unit	Total Sensitivity (%)	Base case	Lower Bound	Upper Bound
1	P_{GF}	Gasification Pressure	bar	28.57	9	5	12
2	$\dot{m}_{sg}$	Syngas Mass Flow rate	kg/s	24.10	50	45	55
3	TIT_{GT}	Gas Turbine Inlet Temperature	°C	21.91	1291	1100	1300
4	$\dot{W}_{net_{GT}}$	Gas Turbine Net Power Generation	MW	17.69	15	13	16
5	$\dot{m}_{LP_{steam}}$	LP Steam Generation	kg/s	14.44	5	3	6
6	n_{WT}	Number of Wind Turbine	–	8.31	35	32	38
7	$r_{P_{AC}}$	Air Compressor Pressure Ratio	–	3.95	13	10	15
8	TIP_{SCO2T}	SCO_2 Turbine Inlet Pressure	°C	1.51	27.32	26	28
9	TIT_{ORCT}	ORC Turbine Inlet Temperature	°C	1.46	123	122	128

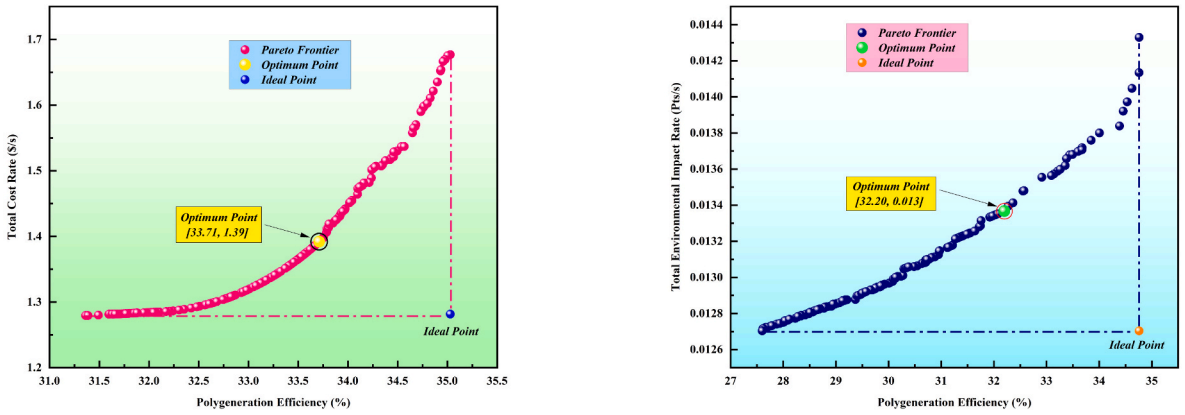

Fig. 11. Pareto charts (a) polygeneration efficiency and total cost rate and (b) polygeneration efficiency and total environmental impact rate.

Table 13
Multi-objective optimization results for all performance parameters of the proposed polygeneration system.

Parameters	*Base case*	*Four objective*	*Improvement (%)*	*Three objective*	*Improvement (%)*
Net power generation (MW)	17.93	17.26	−3.74	18.51	3.23
Net ammonia flow rate production (ton/day)	297.86	256.25	−13.97	275.44	7.53
Mass flow rate of LP steam generation (kg/s)	5	5.11	2.20	3.17	−36.60
Mass flow rate of oxygen generation (ton/day)	52.30	64.83	23.96	63.74	21.87
Overall polygeneration efficiency (%)	31.33	30.94	−1.24	31.87	1.72
Total exergy destruction (MW)	553.31	524.36	5.23	514.97	6.93
Overall polygeneration exergy efficiency (%)	38.53	26.26	−31.85	28.12	−27.02
Total cost rate of polygeneration system ($/hr)	5631.22	4966.86	11.80	4738.09	15.86
Total environmental impact rate of polygeneration system (Pts/hr)	53.16	48.87	8.07	48.98	7.86
Levelized cost of electricity ($/MWh)	0.05	0.04	20.00	0.04	20.00
Levelized cost of ammonia production ($/kg)	0.06	0.06	0.00	0.06	0.00
Payback Period (year)	3.29	3.26	0.91	2.99	9.12
Net present value (Million USD)	682.41	590.04	−13.54	644.57	−5.55
Internal Rate of Return (IRR) of the system (%)	30	30	0.00	30	0.00
Levelized environmental impact of electricity (mPts/kWh)	2.79	2.67	4.30	2.49	10.75
Levelized environmental impact of ammonia production (mPts/kg)	1.55	1.64	5.81	1.55	0.00
MSW mass flow rate consumption (kg/s)	9.38	8.47	9.70	8.46	9.81
Geothermal mass flow rate consumption (kg/s)	1.67	1.58	5.39	1.43	14.37
Number of wind turbines (model: LTW77)	35	32	8.57	32	8.57
Area of PTC (model: ET-100) in the solar field (Hectares)	13.12	12.26	6.55	10.80	17.68

dragonfly algorithm.

The Firefly algorithm is recognized as a novel algorithm compared to conventional algorithms. It is an innovative algorithm inspired by the natural behavior of fireflies in nature. Moreover, this algorithm exhibits suitable speed and accuracy, as confirmed in the study by Mousavi Rabeti et al. [49]., where its application for energy systems has been validated.

Table 12 presents the results of optimizing three and four objectives. According to this table, in the four-objective optimization scenario, both the total environmental impact rate and the total cost rate have improved, while the polygeneration efficiency has decreased compared to the initial state. The reason for this is that in the current study, the optimal point is selected as the closest point to the ideal point (as depicted in Fig. 11), which, according to the objective functions, represents the most optimal point. In the three-objective optimization, all objective functions have improved compared to the base case. Additionally, Fig. 11 illustrates the Pareto charts along with the optimal point and the ideal point.

The results obtained from the optimization of three and four objectives were evaluated for the overall analysis of the system, and they were compared with the results without optimization in Table 13. According to Table 13, it can be observed that the three-objective optimization yielded better performance for the proposed system, as the improvement in system parameters compared to the four-objective optimization is greater. It is noteworthy that the total cost rate, total environmental impact rate, and MSW mass flow rate have improved by 15.86 %, 7.86 %, and 9.81 %, respectively. This not only indicates better performance with three-objective optimization but also demonstrates the satisfactory performance of the particle swarm optimization algorithm.

The results of the 4E analysis after optimization are presented in the block flow diagram shown in Fig. 12. The energy consumption of the ASU and CO_2 capture process is detailed as follows. The ASU requires 1.38 MW of electricity to produce the nitrogen needed for the ammonia synthesis process. This value is clearly depicted in the block flow diagram (Fig. 12). The CO_2 capture process is integrated within the ammonia synthesis unit as part of a consolidated package that includes an expander (generating power from syngas), the WGS process, CO_2 capture, and ammonia synthesis. Together, this package achieves a net power output of 8.85 MW, balancing its internal energy demands. The CO_2 capture process, due to its relatively low energy requirement compared to the other components, has not been shown separately in the block flow diagram but remains an essential element of the APU's functionality. This integrated approach highlights the system's design logic, where each component is synergistically connected to enhance energy efficiency and process performance. It is also worth mentioning that the proposed polygeneration system includes dynamic systems such

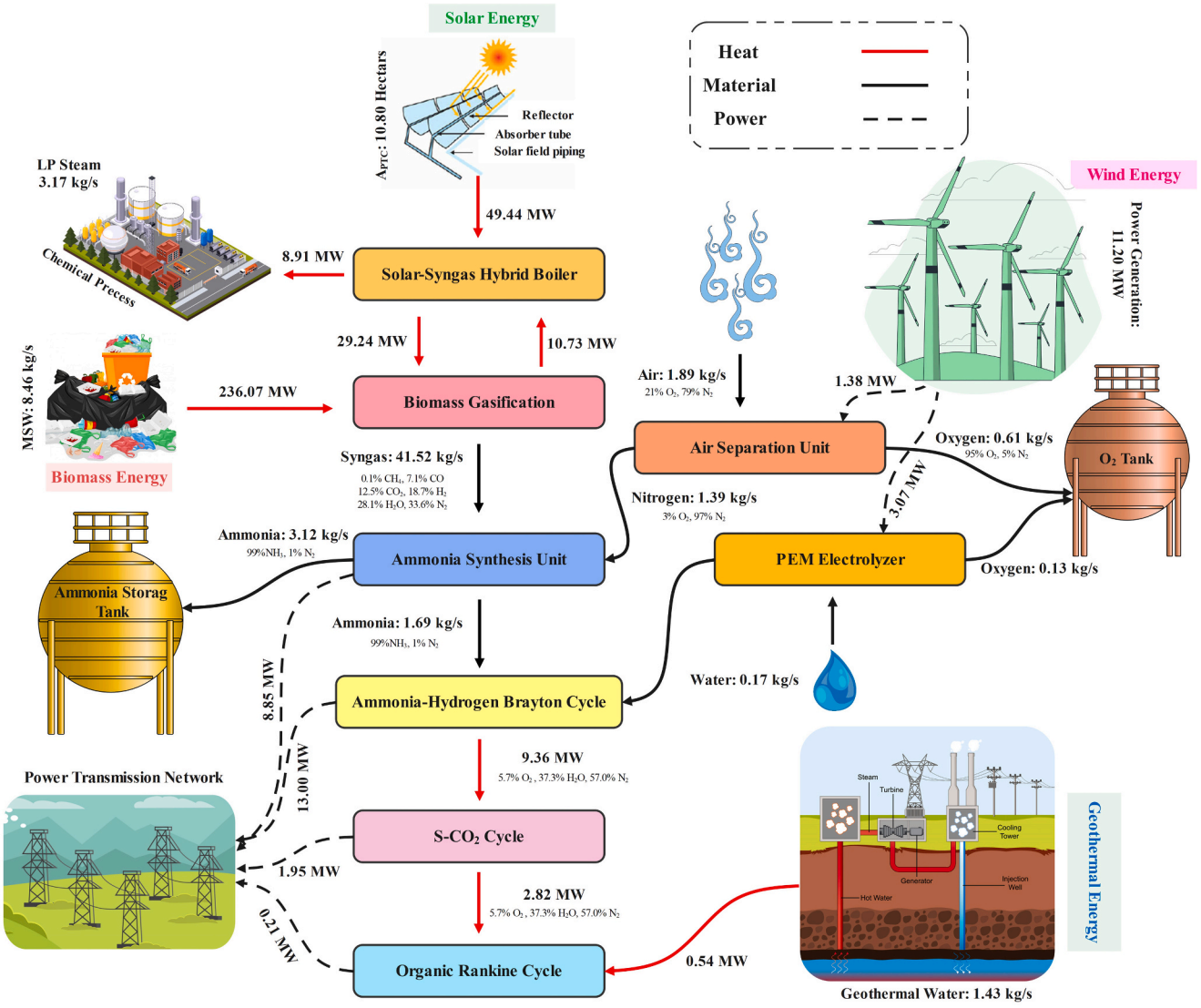

Fig. 12. Block flow diagram of the proposed polygeneration system

as PTC and wind turbines, and the system may experience instability in product generation due to weather fluctuations. Several solutions exist to address this issue. One approach is to incorporate storage systems into the proposed system. This involves storing energy during peak energy times and utilizing it during energy scarcity periods. For the solar part of the system, phase change materials (PCM) can be employed, while battery storage systems can be utilized for the wind part of the system. Another approach is to design the system considering dynamic analysis. For instance, the wind section of the system can be designed based on the minimum wind speed, and by setting a reliability coefficient, the number of wind turbines can be increased to ensure that the system operates smoothly even during low wind conditions (this approach has been considered for the proposed system). Additionally, for the solar part, measures can be taken to allow the system to continue operating independently of this component. As evident from the system schematic, in the present work, the boiler can operate without PTC, and when solar radiation is inadequate, the system can continue functioning by reducing the production of LP steam and increasing the amount of fuel consumed in the boiler. From a developmental perspective, since conventional subsystems such as PEMEC, ASU, ORC, etc., have been utilized in the proposed system, the development of the proposed system does not pose any specific complexities. Although some units like PEMEC and ASU entail numerous equipment and occupy substantial space, they are fully industrialized and operational, capable of playing a significant role in the system. Moreover, while the maintenance and repair of these systems may present challenges, advancements in technology in this field have significantly reduced the need for maintenance and repair. For example, in PEMEC, membranes have improved, and materials used to reduce corrosion and rust in equipment such as boilers have advanced, indicating an improvement in the performance and lifespan of these equipments for use in similar systems.

5. Conclusion

The present work evaluates the design of a novel solar-biomass-wind driven polygeneration system to produce power, process steam, and ammonia from the point of view of energy, exergy, exergeoeconomic, and exergoenvironmental analyses. The innovative nature of this system lies in its integration of multiple renewable energy sources, which enhances overall performance and sustainability. Process steam was produced using a solar-syngas hybrid boiler. Ammonia in the system was created from syngas and nitrogen feeds that are produced from the gasification unit and the air separation unit, respectively. Water gas shifting and CO_2 capture processes were considered to purify the syngas feed of the ammonia synthesis unit. Power generation in the system was created by integrating the ammonia-hydrogen cycle, supercritical

carbon dioxide cycle, and organic Rankine cycle. Wind energy has been used to generate power for the air separation unit and PEM electrolyzer. Geothermal energy was used to preheat the organic fluid entering the turbine in the organic Rankine cycle. Biomass energy was used to supply syngas in the gasification unit with air and steam agents. Solar energy has created part of the process steam heat through parabolic trough collectors.

To model the proposed system from the point of view of energy, the application of machine learning in combination with genetic programming has been used in the gasification unit, ammonia synthesis unit, and air separation unit, representing a significant advancement in modeling efficiency. Finally, the four and three-objective optimization of the proposed system has been done using the dragonfly algorithm. The results of the whole system showed that the overall energy efficiency, overall exergy efficiency, total cost rate, and total environmental impact rate are 31.33 %, 38.53 %, 1.56 $/s, and 14.77 mPts/s, respectively. Ammonia, process steam, and net power production of the whole system were calculated in optimal state 275.44 tons/day, 3.17 kg/s, and 18.51 MW. The payback period of the optimal system was also evaluated as 2.99 years.

Other important results obtained from the analysis of the system are presented as follows:

- Among the used sections, the air separation unit has more destruction and irreversibility.
- The investment cost rate of the solar section is higher than other used units.
- The S-CO_2 turbine has created the greatest environmental impact compared to other equipment.
- The net present value of the whole system is calculated at 682.41 million USD.
- Levelized cost of electricity of the presented system is 0.05 $/kWh.
- The three-objective optimization has created a better improvement for the polygeneration system.
- The three-objective optimization of the system improved overall energy efficiency and total cost rate by 1.72 % and 15.86 %, respectively.
- Gasification pressure is the most sensitive parameter of the presented system.

Future studies could focus on analyzing the proposed system dynamically in response to changes in meteorological data, as this would provide deeper insights into its performance under real-world conditions. Incorporating a storage system could significantly enhance the system's stability and reliability. Additionally, exploring the feasibility of using various biomass fuels would help identify the most suitable options for the proposed system. Advanced control techniques, such as model predictive control (MPC) or AI-driven optimization, could also be integrated to optimize performance under different operational scenarios. Further, using the Monte Carlo method to assess the system's reliability dynamically would provide valuable insights into its robustness. Lastly, given its low environmental impact and potential for biofuel production, the proposed system represents a promising solution for the future of sustainable energy systems. With its enhanced sustainability and innovative design, it can be considered an attractive polygeneration system.

CRediT authorship contribution statement

Mohammad Hasan Khoshgoftar Manesh: Writing – review & editing, Validation, Software, Methodology, Investigation, Conceptualization. **Soheil Davadgaran:** Writing – original draft, Visualization, Software, Methodology, Investigation, Formal analysis. **Seyed Alireza Mousavi Rabeti:** Writing – original draft, Visualization, Validation, Software, Methodology, Investigation, Formal analysis, Conceptualization. **Ana M. Blanco-Marigorta:** Writing – review & editing, Resources, Methodology, Investigation.

Declaration of competing interest

The authors declare that they have no known competing financial interests or personal relationships that could have appeared to influence the work reported in this paper.

Acknowledgments

This research has been co-funded by ERDF funds, INTERREG MAC 2014–2020 programme, within the ACLIEMAC project (MAC2/3.5b/380). No funding sources had any influence on study design, collection, analysis, or interpretation of data, manuscript preparation, or the decision to submit for publication.

Appendix A. Appendix.

Table A1
Mass and energy conservations of all components in the proposed polygeneration system.

Component	Relationships	Known parameters	Unknown Parameters
Boiler	$\dot{Q}_{Boiler_{water}} = \sum_{i=1}^{n}\left(\dot{m}_{out}h_{out}\right)_i - \sum_{i=1}^{n}\left(\dot{m}_{In}h_{In}\right)_i$ $\dot{Q}_{Boiler_{Fluegas}} = \frac{\dot{Q}_{Boiler_{water}}}{\eta_{Boiler}}$ $\dot{Q}_{Boiler_{Fluegas}} = \dot{m}_f LHV_f + \dot{m}_a h_a - \dot{m}_{fg}h_{fg}$ $\dot{m}_a + \dot{m}_f = \dot{m}_{fg}$	η_{Boiler} $\dot{m}_{out}$ $\dot{m}_{In}$ $T_a P_a$ $T_{fg} P_{fg}$ $LHV_f T_{out} P_{out}$ $T_{In} P_{In}$	$\dot{m}_f$ $\dot{m}_a$
Turbines Expander	$h_{In} = h(T_{In}.P_{In}).s_{In} = s(T_{In}.P_{In})$ $\eta_T = \frac{h_{In} - h_{Out}}{h_{In} - h_{Out_s}} h_{Out_s} = h(P_{Out}.S_{In})$ $\dot{W}_T = \dot{m}_T(h_{In} - h_{Out})$	T_{In} P_{In} η_T $\dot{m}_T$ P_{Out}	$\dot{W}_T$
Compressors	$h_{In} = h(T_{In}.P_{In}).s_{In} = s(T_{In}.P_{In})$ $\eta_C = \frac{h_{Out_s} - h_{In}}{h_{Out} - h_{In}} h_{Out_s} = h(P_{Out}.S_{In})$ $\dot{W}_C = \dot{m}_C(h_{Out} - h_{In})$	T_{In} P_{In} η_C	$\dot{W}_C$

(*continued on next page*)

Table A1 (*continued*)

Component	Relationships	Known parameters	Unknown Parameters
Combustion cahmber	$AF = \frac{\dot{m}_a}{\dot{m}_f}$ $\dot{m}_a h_a + \dot{m}_f LHV_f = \dot{m}_{fg} h_{fg} \dot{m}_a + \dot{m}_f = \dot{m}_{fg}$	$\dot{m}_C$ P_{Out} $T_a P_a$ $T_{fg} P_{fg}$ LHV_f $\dot{m}_a$ T_{In} P_{In}	AF $\dot{m}_f$ $\dot{m}_{fg}$
Pumps	$h_{In} = h(T_{In}.P_{In})$ $s_{In} = s(T_{In}.P_{In})$ $\eta_P = \frac{h_{Out_s} - h_{In}}{h_{Out} - h_{In}}$ $h_{Out_s} = h(P_{Out}.S_{In})$ $\dot{W}_P = \dot{m}_P(h_{Out} - h_{In})$	η_P $\dot{m}_P$ P_{Out}	$\dot{W}_P$
Heat exchangers	$h_{Hot.in} = h(T_{Hot.in}.P_{Hot.in})$ $h_{Hot.out} = h(T_{Hot.out}.P_{Hot.out})$ $h_{Cold.in} = h(T_{Cold.in}.P_{Cold.in})$ $h_{Cold.out} = h(T_{Cold.out}.P_{Cold.out})$ $\dot{Q}_{Hot} = \dot{m}_{Hot}(h_{Hot.in} - h_{Hot.out})$ $\dot{Q}_{Cold} = \dot{m}_{Cold}(h_{Cold.out} - h_{Cold.in})$ $\dot{Q}_{Hot} = \dot{Q}_{Cold}$	$T_{Hot.in}$ $P_{Hot.in}$ $T_{Hot.out}$ $P_{Hot.out}$ $T_{Cold.in}$ $P_{Cold.in}$ $T_{Cold.out}$ $P_{Cold.out}$ $\dot{m}_{Hot}$	$\dot{m}_{Cold}$ $\dot{Q}_{HX}$
PEM Elrctrolyzer [74]	$\dot{N}_{H_2,out} = \frac{J}{2F} = \dot{N}_{H_2O,\ reacted}$ $\dot{N}_{O_2,out} = \frac{J}{4F}$ $\dot{N}_{H_2O,\ out} = \dot{N}_{H_2O,\ in} - \frac{J}{2F}$ $\dot{E}_{electric} = JV$ $V = V_o + \eta_{act,\ a} + \eta_{act,\ c} + \eta_{ohm}$ $\sigma[\lambda(x)] = [0.5139\,\lambda(x) - 0.326]exp\left[1268\left(\frac{1}{303} - \frac{1}{T}\right)\right]$ $\lambda(x) = \frac{\lambda_a - \lambda_c}{L}x + \lambda_c$ $R_{pem} = \int_0^L \frac{dx}{\sigma[\lambda(x)]}$ $\eta_{ohm} = JR_{pem}$ $\eta_{act,i} = \frac{RT}{F} sinh^{-1}\left(\frac{J}{2J_{o,\ i}}\right) \qquad i = a,c$ $J_{o,\ i} = J_i^{ref} exp\left(-\frac{E_{act,i}}{RT}\right) \qquad i = a,c$	$\dot{E}_{electric}$ A_{PEM} $\dot{N}_{H_2O,\ reacted}$	$\dot{N}_{H_2,out}$ $\dot{N}_{O_2,out}$ N_{pem}
PTC filed ET-100 [83]	$Q_{solar} = A_{coll} DNI$ $Q_u = \dot{m}_{HTF} c_p (T_{out} - T_{in}) = \eta_c \times Q_{solar}$ $\eta_c = 0.75 - 0.000045(T_{in} - T_{out}) - 0.039\left(\frac{T_{in} - T_{out}}{DNI}\right) - 0.0003\,DNI\left(\frac{T_{in} - T_{out}}{DNI}\right)^2$	T_{out} T_{in} $\dot{m}_{HTF}$ c_p DNI	A_{coll} Q_u Q_{solar}
Air-steam Gasification	$y_{cH_4} = 0.340H^2 + 0.002P_G C^2 + 0.0007CP_G{}^2 MC^2 - 0.0004 - 0.016P_G HO - 0.521CH^2$ $y_{CO} = 0.092 + 0.079H + 0.016O - 0.0004P_G - 0.018C - 0.131N - 0.168MC$ $y_{CO_2} = 0.115 + 0.150C + 0.043MC + 0.0002P_G - 0.030O - 0.905H$ $y_{H_2} = 0.156 + 0.619H + 0.192C - 0.041N - 0.2O - 0.851CH$ $y_{H_2O} = 0.249 + 0.472O + 0.397H + 0.330MC - 0.052N - 0.420C$ $y_{N_2} = 0.357 + 0.264H + 0.152C + 0.114N - 0.206MC - 0.252O$ $T_G = 861.126 + 2536.553H + 915.683O - 2.572P_G - 412.292MC - 424.420N - 1051.946C$ $\dot{m}_{Biomass} = 0.280\dot{m}_{Syngas} - 0.072\dot{m}_{Syngas} C - 0.263\dot{m}_{Syngas} MC - 0.435\dot{m}_{Syngas} H$ $\dot{m}_{Steam} = 0.750 - 0.132\dot{m}_{Syngas} + 0.209\dot{m}_{Syngas} O - 0.138\dot{m}_{Syngas} MC - 21.072CH$ $\dot{m}_{Air} = 0.110 + 4.437H + 0.773C + 0.114\dot{m}_{Syngas} - 1.154MC - 1.542N - 1.717O$	MC H C O N P_G $\dot{m}_{Syngas}$	y_{cH_4} y_{CO} y_{CO_2} y_{H_2} y_{H_2O} T_G $\dot{m}_{Biomass}$ $\dot{m}_{Steam}$ $\dot{m}_{Air}$
Ammonia synthises production unit	$\dot{m}_{Ammonia}(kg/h) = 2074.670 \times \dot{m}_{Syngas} y_{H_2} + 3347.600 \times \dot{m}_{Syngas} y_{H_2} y_{H_2O} - 285.787 - 136.520 \times \dot{m}_{Syngas}$ $m_{Amine}\ (kg/h) = 612.325 \times 10^4 + 0.201 \times \dot{m}_{Syngas} + 4883.110 \times \dot{m}_{Syngas} y_{CO} + 4600.613 \times \dot{m}_{Syngas} y_{CO_2} + 0.261 \times \dot{m}_{Syngas} y_{H_2O} - 403.245 \times \dot{m}_{Syngas} - 34.667 \times 10^3 \times y_{N_2} - 37.634 \times 10^3 \times y_{H_2O}$ $\dot{m}_{out_w}(kg/s) = 2.010 + 305.253 \times \dot{m}_{Syngas} + 2932.104 \times \dot{m}_{Syngas} y_{H_2O} + 245.408 \times \dot{m}_{Syngas} y_{H_2} - 0.108 \times \dot{m}_{Syngas} - 2775.025 \times \dot{m}_{Syngas} y_{CO}$ $\dot{W}_{ASPU}(kW) = 432.038 \times \dot{m}_{Syngas} + 239.865 \times T_{syngas} \times \frac{\dot{m}_{Syngas}}{P_{syngas}} - 20.284 - 0.418 \times P_{syngas} \dot{m}_{Syngas} + 44.246 \times 10^3 y_{H_2} + 0.737 \times \dot{m}_{Syngas} + 116.702 \times T_{syngas} \times y_{H_2} + 44.246 \times 10^3 \times y_{N_2}^2 - 29.348 \times 10^3 - 1.947 \times P_{syngas} \times \dot{m}_{Syngas}{}^* cos(0.064 \times P_{syngas})$ $\dot{Q}_{ASPU}(kJ/hr) = 566.424 \times 10^4 \times \dot{m}_{Syngas} y_{CO} - 4207.978 - 623.067 \times 10^3 \times \dot{m}_{Syngas} - 721.640 \times 10^3 \times \dot{m}_{Syngas} y_{N_2} - 371.345 \times 10^4 \times \dot{m}_{Syngas} y_{H_2} - 909.099 \times 10^4 \times \dot{m}_{Syngas} y_{H_2O} + 161.582 \times 10^4 + 460.749 \times \dot{m}_{Syngas} + 244.295 \times 10^4 \times \dot{m}_{Syngas} y_{H_2O} - 128.163 \times 10^3 \times \dot{m}_{Syngas} y_{H_2} - 564.096 \times 10^5 \times \dot{m}_{Syngas} y_{CO} y_{H_2O} + 144.963 \times 10^4 \times \dot{m}_{Syngas} + 288.174 \times \dot{m}_{Syngas} y_{CO} + 226.247 \times 10^4 \times \dot{m}_{Syngas} y_{H_2} - 105.427 \times 10^4 \times \dot{m}_{Syngas} y_{H_2O} + 595.481 \times 10^5 + 608.723 \times 10^3 \times \dot{m}_{Syngas} + 605.258 \times \dot{m}_{Syngas} y_{N_2} - 723.437 \times 10^5 y_{H_2O} - 871.572 \times 10^5 \times y_{N_2} - 119.444 \times 10^6 y_{CO_2}$	y_{cH_4} y_{CO} y_{CO_2} y_{H_2} y_{H_2O} $\dot{m}_{Syngas}$ P_{syngas} T_{syngas}	$\dot{m}_{Ammonia}$ m_{Amine} $\dot{m}_{out_w}$ $\dot{W}_{ASPU}$ $\dot{Q}_{ASPU}$
Air Separation Unit [78]	$\dot{W}_{net}\ (W) = 284.293 \times 10^3 + 143.601 \times 10^5 \times \dot{n}_{Air} + 1728.169 \times \dot{n}_{Air} \times P_{N_2} + 344.853 \times \dot{n}_{Air} \times P_{O_2}$ $\dot{Q}_{inter\ cooler}\ (W) = 171.600 \times 10^4 + 964.363 \times 10^4 \times \dot{n}_{Air} + 2777.423 \times \dot{n}_{Air} \times P_{N_2} + 734.082 \times P_{O_2} \times \dot{n}_{Air} + 297.397 \times \dot{n}_{Air} \times P_{O_2} - 918.654 \times P_{N_2}$ $\dot{Q}_{cooling_{sepration}}(W) = 416.666 \times 10^4 + 79.880 \times 10^3 \times T_{Air} \times \dot{n}_{Air} + 14.895 \times 10^3 \times T_{Air}^2 - 606.849 \times 10^3 \times T_{Air}$	$\dot{n}_{Air}$ P_{O_2} P_{N_2} T_{Air}	$\dot{W}_{net}$ $\dot{Q}_{inter\ cooler}$ $\dot{Q}_{cooling_{sepration}}(W)$ $\dot{Q}_{heating_{sepration}}$

(*continued on next page*)

Table A1 (*continued*)

Component	Relationships	Known parameters	Unknown Parameters
	$\dot{Q}_{heating_{seprarion}}(W) = 512.348 \times 10^4 \times \dot{n}_{Air} + 15.979 \times 10^3 \times T_{Air}^2 - 163.609 \times 10^5 - 101.033 \times 10^3 \times T_{Air} \times \dot{n}_{Air}$		$\dot{m}_{O_2}$
	$\dot{m}_{O_2} = 0.332 + 6.706 \times \dot{n}_{Air} + 0.053 \times \dot{n}_{Air}^3 + 0.335 \times \dot{n}_{Air} \times \left(0.285 \times \dot{n}_{Air}^{\dot{n}_{Air}} - 0.005 \times \dot{n}_{Air}^5\right.$		$\dot{m}_{N_2}$
	$\dot{m}_{N_2} = 22.142 \times \dot{n}_{Air} + \frac{0.393}{\dot{n}_{Air}^{\dot{n}_{Air}}} + 0.0001 \times \dot{n}_{Air} \times \dot{n}_{Air}^{\dot{n}_{Air}} - 0.650 - 0.015 \times \dot{n}_{Air}^{\dot{n}_{Air}} \times 0.117^{0.003 \times \dot{n}_{Air} \times \dot{n}_{Air}^{\dot{n}_{Air}}}$		$T_{N_2\,Out}$
	$T_{N_2\,Out} = 2.090 \times P_{N_2} + 500.951 \times \frac{10^3}{P_{N_2}} + 1.203 \times 10^{-7} \times P_{N_2}^3 - 1719.681 - 0.0009 \times P_{N_2}^2$		$T_{O_2\,Out}$
	$T_{O_2\,Out} = 3448.066 + -329.317 \times 10^4 / P_{O_2} + 0.0002 \times P_{O_2}^2 + 106.918 \times 10^7 / P_{O_2}^2 + 547.631 \times$		
	$10^{12} / \left(307.023 \times 10^{11} - \times P_{O_2}^4\right) - 1.347 \times P_{O_2} - 2.385 \times 10^{-16} \times P_{O_2}^5$		
	$V = V_{ref} \times \left(\frac{h}{h_{ref}}\right)^{\alpha}$		
Wind Turbines [72]	$\dot{W}_{WT} = \frac{1}{2} C_p \rho A V^3$	$\dot{W}_{WT}$	n_{WT}
	$\dot{W}_{WT,total} = n_{WT} \times \dot{W}_{WT}$		

Table A2
Cost and weight relationships of all component in the present study [85]

Component	Cost equations ($)	Weight equations (ton)
Compressors	$PEC = 71.1 \times \frac{\dot{m}}{0.92 - \eta_C} \times r_p \times \ln(r_p)$	$\rho = \frac{P_o}{R \times T_o}.A = \frac{\dot{m}}{\rho \times vel}.D = \sqrt{\frac{4}{\pi \times A}}.Weight = \frac{P_o \times D \times FS}{2 \times \sigma}$
CC	$PEC = 46.08 \times \frac{\dot{m}_a^{\bullet}}{0.995 - \frac{P_o}{P_i}} \times (1 + \exp.(0.018 \times T_o - 26.4))$	$\rho = \frac{P_o}{R_{fg} \times T_o}.A = \frac{\dot{m}_{fg}^{\bullet}}{\rho \times vel}.D = \sqrt{\frac{4}{\pi \times A}}.Weight = \frac{P_o \times D \times FS}{2 \times \sigma}$
ACC	$PEC = 1773 \dot{m}_{Cooled\ Fluid}$	$Weight = 0.073 \left(\frac{\dot{Q}_{Cond}}{1000}\right)^{0.99}$
OFOHs	$PEC = 145315 \times \left(\dot{m}_{ORC}\right)^{0.7}$ [95]	$Weight = 2.49 \times \left(\dot{m}_{ORC}\right)^{0.7}$
GT/SCO_2T	$PEC = 479.34 \times \frac{\dot{m}_{fg}^{\bullet}}{0.93 - \eta_{GT}} \times \ln\left(\frac{P_i}{P_o}\right) \times (1 + \exp.(0.036 \times T_i - 54.4))$	$\rho = \frac{P_o}{R_{fg} \times T_o}.A = \frac{\dot{m}_{fg}^{\bullet}}{\rho \times vel}.D = \sqrt{\frac{4}{\pi \times A}}.Weight = \frac{P_o \times D \times FS}{2 \times \sigma}$
Gasifier	$PEC = 1600 \times \left(\dot{m}_{Bio} \times 3600\right)^{0.67}$ [96]	$\rho = \frac{P_o}{R_{sg} \times T_o}.A = \frac{\dot{m}_{fg}^{\bullet}}{\rho \times vel}.D = \sqrt{\frac{4}{\pi \times A}}.Weight = \frac{P_o \times D \times FS}{2 \times \sigma}$
HXs	$PEC = 235 \times \dot{Q}_{Hx}^{0.75}$ [97]	$Weight = 2.14 \times \left(\frac{\dot{Q}_{Hx}}{1000}\right)^{0.7}$
ORCP	$PEC = 2100 \left(\frac{\dot{W}_{ORCP}}{10}\right)^{0.26} \times \left(\frac{1 - \eta_{ORCP}}{\eta_{ORCP}}\right)^{0.5}$	$Weight = 0.0061 \times \dot{W}_{ORCP}^{0.95}$
OPCT	$PEC = \frac{497.34 \dot{m}_{ORC} ln\left(\frac{P_1}{p_2}\right)}{0.92 - \eta_{ORCT}} (1 + exp(0.036 T_1 - 54.4))$ [98]	$Weight = 4.9 \times \dot{W}_{ORCT}^{0.7}$
PEMEC	$PEC = 1000 \dot{W}_{PEM}$ [60]	$Weight = 0.0146 \times \dot{W}_{PEM}$ [83]
PTCs	$PEC = 355 \times A_{SF}$	$Weight = 0.019 \times A_{SF}$ [99]
Pumps	$PEC = 2100 \left(\frac{\dot{W}_P}{10}\right)^{0.26} \times \left(\frac{1 - \eta_P}{\eta_P}\right)^{0.5}$	$Weight = 0.0061 \times \dot{W}_P^{0.95}$
Boiler	$PEC = a_1 \times \dot{m}_{Boiler}^{a_2} \times \phi_p \times \phi_t \times \phi_\eta \times \phi_{\frac{SH}{RSH}}$ $\phi_p = exp\left(\frac{P_e - \overline{P}_e}{a_3}\right)$ $\phi_t = 1 + a_5 exp\left(\frac{T_e - \overline{T}_e}{a_6}\right)$ $\phi_\eta = 1 + \left(\frac{1 - \overline{\eta}_1}{1 - \eta_1}\right)^{a_4}$ $\phi_t = 1 + \frac{T_e - T_{iSH}}{T_e} + \frac{\dot{m}_{RSH}}{\dot{m}_{Boiler}} \times \frac{T_{eRSH} - T_{iRSH}}{T_{eRSH}}$ $\overline{T}_e = 593^{\circ}C \quad \overline{P}_e = 28\ bar \quad \overline{\eta}_1 = 0.9$ $a_1 = 2.8582\ \$\ kg^{-1}s^{-1} \quad a_2 = 0.8$ $a_3 = 150\ bar \quad a_4 = 7$ $a_5 = 5 \quad a_6 = 10.42^{\circ}C$ [100]	$Weight = \frac{100 P_{out} \times D \times FS}{2\sigma}$ $FS = 1.6 \quad v = 6.2 \frac{m}{s} \quad \sigma = 45.6$ [100]
Reactors	$PEC = 6852 \times \dot{m}$ [101]	$Weight = 8.050 \times V_{Rector}$
columns	$C_t = 457.7 \times exp(0.1739D)$ $C_b = 1.28 \times exp\left(6.629 + 0.1826 \times log(Weight) + 0.02297 \times (log(Weight))^2\right)$ $C_p = 300 D^{0.7396} \times (T_s \times n)^{0.7068}$ $PEC = 1.218 \times (C_b + n \times C_t + C_p)$ [102]	$Weight = 8.050 \times V_{Column}$

(*continued on next page*)

Table A2 (*continued*)

Component	Cost equations ($)	Weight equations (ton)
ASU	$\text{PEC} = (\text{Ref Cost}) \times \left(\frac{\text{Size}}{\text{Ref Size}}\right)^{\text{Scalling Exponent}} \times (\text{Overall Instalation Factor})$ Scalling Exponent = 0.5 Overall Instalation Factor = 1 Ref Cost = 141 Million US$ Ref Size = 52 kg O_2/s [103]	$\text{Weight} = 0.0061 \times \dot{W}_{ASU}^{0.95}$ [103]
WT	$\text{PEC} = 3090 \times \dot{W}_{WT}$	$\text{Weight} = 0.26 \times \dot{W}_{WT}^{0.95}$

Table A3
Stream table of proposed system.

No.	Fluid	$\dot{m}$ (kg/s)	$T(^{\circ}C)$	P (bar)
1	Water	16.43	25.00	1.013
2	Water	16.43	25.01	3.00
3	Air	15.20	25.00	1.013
4	Water	16.43	133.52	3.00
5	Water	16.43	133.56	5.10
6	Water	5.00	133.56	5.10
7	Water	5.00	151.83	5.00
8	Water	5.00	180.00	5.00
9	Water	11.43	133.56	5.10
10	Water	11.43	133.62	9.18
11	Water	11.43	175.35	9.00
12	HTF	201.08	225.35	2.94
13	HTF	201.08	163.62	3.00
14	HTF	142.50	163.55	3.00
15	HTF	142.50	201.83	2.94
16	Water	11.43	200.00	9.00
17	Air	5.68	175.35	9.00
18	MSW	9.38	25.00	1.013
19	Syngas	50.00	779.13	9.00
20	Syngas	4.34	779.13	9.00
21	Syngas	45.66	779.13	9.00
22	Syngas	45.66	643.83	4.50
23	Mixture	33.26	450.00	14.40
24	Carbon dioxide	11.23	35.00	12.00
25	Mixture	22.03	35.86	14.40
26	Ammonia	5.35	−3.33	30.00
27	Ammonia	3.45	−3.33	30.00
28	Ammonia	1.90	−3.33	30.00
29	Water	0.19	25.00	1.00
30	Hydrogen	0.02	80.00	1.00
31	Oxygen	0.15	80.00	1.00
32	Air	12.28	25.00	1.013
33	Air	12.28	374.33	13.17
34	Flue gas	14.20	1291.00	13.17
35	Flue gas	14.20	704.87	1.08
36	Flue gas	14.20	212.08	1.04
37	S-CO_2	31.76	378.90	273.20
38	S-CO_2	31.76	260.05	88.04
39	S-CO_2	31.76	86.19	87.62
40	S-CO_2	31.76	36.85	87.20
41	S-CO_2	31.76	79.27	276.00
42	S-CO_2	31.76	192.08	274.60
43	Flue gas	14.20	120.00	1.013
44	R123	9.48	123.00	12.01
45	R123	7.61	63.02	1.55
46	R123	7.61	44.90	1.55
47	R123	7.61	40.04	1.55
48	R123	7.61	40.31	5.81
49	R123	7.61	53.03	5.81
50	R123	1.86	97.98	5.81
51	R123	9.48	87.00	5.81
52	R123	9.48	87.54	12.01
53	Water	1.67	110.00	9.00
54	Water	1.67	110.00	10.00
55	Water	1.67	90.00	10.00
56	Air	158.58	25.00	1.013
57	Air	158.58	35.00	1.013
58	Air	1.88	25.00	1.013
59	Oxygen	0.49	122.74	12.00
60	Nitrogen	1.39	149.74	12.00

Data availability

Data will be made available on request.

References

[1] Babaelahi M, Rafat E, Mofidipour E. Emergy-based economic and environmental analysis and multi-objective optimization of a two-cascade solar gas turbine power plant. Sustainable Production and Consumption 2019;20:165–77.
[2] Fayyazbakhsh A, et al. Engine emissions with air pollutants and greenhouse gases and their control technologies. J Clean Prod 2022;376:134260.
[3] Mousavitabar SMA, Manesh MHK. Multi-objective optimization and 4E analysis of a novel stand-alone LNG production system by employing the machine-learning approach. Fuel 2024;374:132415.
[4] Kasaeian A, et al. Solar-driven polygeneration systems: Recent progress and outlook. Appl Energy 2020;264:114764.
[5] Manesh MHK, Davadgaran S, Rabeti SAM. Experimental study of biological wastewater recovery using microbial fuel cell and application of reliability and machine learning to predict the system behavior. Energy Convers Manag 2024;314:118658.
[6] Malode SJ, et al. Recent advances and viability in biofuel production. Energy Conversion and Management: X 2021;10:100070.
[7] Joshi G, et al. Challenges and opportunities for the application of biofuel. Renew Sust Energ Rev 2017;79:850–66.
[8] Yuksel YE, Ozturk M, Dincer I. Development and assessment of a biomass-gasification based multigenerational plant for production of hydrogen and ammonia fuels. Fuel 2025;380:133187.
[9] Wan Z, et al. Ammonia as an effective hydrogen carrier and a clean fuel for solid oxide fuel cells. Energy Convers Manag 2021;228:113729.
[10] Oni A, et al. Comparative assessment of blue hydrogen from steam methane reforming, autothermal reforming, and natural gas decomposition technologies for natural gas-producing regions. Energy Convers Manag 2022;254:115245.
[11] Ishaq H, Dincer I. Investigation and optimization of a new hybrid natural gas reforming system for cascaded hydrogen, ammonia and methanol synthesis. Comput Chem Eng 2021;148:107234.
[12] Zhang J, et al. A novel power, DME, and ammonia polygeneration system using Aspen plus based on the integration of biomass gasification and syngas chemical looping. Energy Convers Manag 2024;299:117808.
[13] Sun S, et al. Ammonia as hydrogen carrier: Advances in ammonia decomposition catalysts for promising hydrogen production. Renew Sust Energ Rev 2022;169:112918.
[14] Lamb KE, Dolan MD, Kennedy DF. Ammonia for hydrogen storage; A review of catalytic ammonia decomposition and hydrogen separation and purification. Int J Hydrog Energy 2019;44(7):3580–93.
[15] Ezzat M, Dincer I. Energy and exergy analyses of a novel ammonia combined power plant operating with gas turbine and solid oxide fuel cell systems. Energy 2020;194:116750.
[16] Ozturk M, Dincer I. An integrated system for ammonia production from renewable hydrogen: a case study. Int J Hydrog Energy 2021;46(8):5918–25.
[17] Huang W, et al. Exergoeconomic and exergoenvironmental analysis of a combined heating and power system driven by geothermal source. Energy Convers Manag 2020;211:112765.
[18] Tukenmez, N., M. Koc, and M. Ozturk, A novel combined biomass and solar energy conversion-based multigeneration system with hydrogen and ammonia generation. Int J Hydrog Energy, 2021. 46(30): p. 16319–16,343.
[19] Sagel VN, Rouwenhorst KH, Faria JA. Green ammonia enables sustainable energy production in small island developing states: A case study on the island of Curaçao. Renew Sust Energ Rev 2022;161:112381.
[20] Campion N, et al. Techno-economic assessment of green ammonia production with different wind and solar potentials. Renew Sust Energ Rev 2023;173:113057.
[21] Razi F, Dincer I. Renewable energy development and hydrogen economy in MENA region: A review. Renew Sust Energ Rev 2022;168:112763.
[22] Dagoumas AS, Koltsaklis NE. Review of models for integrating renewable energy in the generation expansion planning. Appl Energy 2019;242:1573–87.
[23] Kumar R, et al. Thermodynamic investigation of water generating system through HDH desalination and RO powered by organic Rankine cycle. Mater Today: Proc 2021;46:5256–61.
[24] Abu-Rayash A, Dincer I. Development and assessment of an integrated wind-solar based energy system for sustainable communities. Energy Convers Manag 2023;277:116680.
[25] Østergaard PA, Duic N, Kalogirou S. Sustainable development using integrated energy systems and solar, biomass, wind, and wave technology. In: Vol. 235. Elsevier; 2024. p. 121359.
[26] Sánchez-Lozano D, et al. Techno-economic assessment of a hybrid PV-assisted biomass gasification CCHP plant for electrification of a rural area in the Savannah region of Ghana. Appl Energy 2025;377:124446.
[27] Yilmaz F. Design and performance analysis of hydro and wind-based power and hydrogen generation system for sustainable development. Sustain Energy Technol Assessments 2024;64:103742.
[28] Yilmaz F, Ozturk M, Selbas R. Design and performance evaluation of a biomass-based multigeneration plant with supercritical CO2 brayton cycle for sustainable communities. Int J Hydrog Energy 2024;59:1540–54.
[29] Cimmino L, Burgos JB, Eicker U. Exergy and thermoeconomic analysis of a novel polygeneration system based on gasification and Power-to-X strategy. Renew Energy 2024;236:121438.
[30] Rabeti SM, Manesh MK, Amidpour M. Techno-economic and environmental assessment of a novel polygeneration system based on integration of biomass air-steam gasification and solar parabolic trough collector. Sustain Energy Technol Assessments 2023;56:103030.
[31] Lin S, et al. Design and Economic Analysis of an Innovative Multi-Generation System in Different Countries with Diverse Economic Contexts. Energy 2024;310:133178.
[32] Rabeti SAM, et al. Development of a New strategy for selecting solar desalination plants based on Techno-Economic, Environmental, and climatic Issues: The case study of Iran. Sustain Energy Technol Assessments 2025;73:104122.
[33] Mehrabian M, Manesh MK. 4E, risk, diagnosis, and availability evaluation for optimal design of a novel biomass-solar-wind driven polygeneration system. Renew Energy 2023;219:119531.
[34] Bersalli G, Menanteau P, El-Methni J. Renewable energy policy effectiveness: A panel data analysis across Europe and Latin America. Renew Sust Energ Rev 2020;133:110351.
[35] Khani N, Manesh MK, Onishi V. 6E analyses of a new solar energy-driven polygeneration system integrating CO2 capture, organic Rankine cycle, and humidification-dehumidification desalination. J Clean Prod 2022;379:134478.
[36] Amidpour M, Man MHK. Cogeneration and Polygeneration Systems. Academic Press; 2020.
[37] Wang D, et al. Optimized multi-criteria performance of a poly-generation layout including a Stirling engine and a supercritical Brayton cycle using biogas and methane as two potential fuels of a topping gas turbine cycle. Energy 2024;310:133172.
[38] Calise F, et al. Polygeneration. In: Polygeneration Systems. Elsevier; 2022. p. 1–33.
[39] Rami Y, Allouhi A. 3 E (Energy, Exergy and Economic) multi-objective optimization of a novel solar-assisted ocean thermal energy conversion system for integrated electricity and cooling production. Energy Convers Manag 2024;321:119006.
[40] Kanberoglu B, et al. The effects of different working fluids on the performance characteristics of the Rankine and Brayton cycles. Int J Hydrog Energy 2024;49:1059–74.
[41] Valera-Medina A, et al. Ammonia, methane and hydrogen for gas turbines. Energy Procedia 2015;75:118–23.
[42] Crespi F, et al. Supercritical carbon dioxide cycles for power generation: A review. Appl Energy 2017;195:152–83.
[43] Tabriz ZH, et al. Enhancing a bio-waste driven polygeneration system through artificial neural networks and multi-objective genetic algorithm: Assessment and optimization. Int J Hydrog Energy 2024;58:1486–503.
[44] Wang T, et al. Poly-generation system with waste heat of low-temperature flue gas in power plants based on organic Rankine cycle. Appl Therm Eng 2024;242:122513.
[45] Manesh MHK, Davadgaran S, Rabeti SAM. New Procedure for Designing an Innovative Biomass-Solar-Wind Polygeneration System for Sustainable Production of Power, Freshwater, and Ammonia Using 6E Analyses, Carbon Footprint, Water Footprint, and Multi-Objective Optimization. Renew Energy 2024:120802.
[46] Ghasemi A, et al. Exergoeconomic and exergoenvironmental analyzes of a new biomass/solar-driven multigeneration energy system: An effort to maximum utilization of the waste heat of gasification process. Thermal Science and Engineering Progress 2024;48:102407.
[47] Manesh MHK, et al. Optimal 4E Evaluation of an Innovative Solar-wind Cogeneration System for Sustainable Power and Fresh Water Production Based on Integration of Microbial Desalination Cell, Humidification-Dehumidification, and Reverse Osmosis Desalination. Energy 2024;297:131256.
[48] Shariati M, et al. Thermodynamic evaluation of a state-of-art poly-generation system fueled by natural gas and biomass for cooling, power, and hot water generation. Thermal Science and Engineering Progress 2024;47:102308.
[49] Rabeti SAM, Manesh MHK, Amidpour M. An innovative optimal 4E solar-biomass waste polygeneration system for power, methanol, and freshwater production. J Clean Prod 2023;412:137267.
[50] Tabriz ZH, et al. Energy, exergy, exergoeconomic, and exergoenvironmental (4E) analysis of a new bio-waste driven multigeneration system for power, heating, hydrogen, and freshwater production: Modeling and a case study in Izmir. Energy Convers Manag 2023;288:117130.
[51] Hashemian N, Noorpoor A. A geothermal-biomass powered multi-generation plant with freshwater and hydrogen generation options: Thermo-economic-environmental appraisals and multi-criteria optimization. Renew Energy 2022;198:254–66.
[52] Safder U, et al. Energetic, economic, exergetic, and exergorisk (4E) analyses of a novel multi-generation energy system assisted with bagasse-biomass gasifier and multi-effect desalination unit. Energy 2021;219:119638.
[53] Ghasemiasl R, et al. Exergetic and economic optimization of a solar-based cogeneration system applicable for desalination and power production. J Therm Anal Calorim 2020;145.
[54] Ehyaei M, et al. Energy, exergy, economic, exergoenvironmental, and environmental analyses of a multigeneration system to produce electricity, cooling, potable water, hydrogen and sodium-hypochlorite. Desalination 2021;501:114902.
[55] Entezari A, et al. Artificial intelligence and machine learning in energy systems: A bibliographic perspective. Energy Strategy Rev 2023;45:101017.

[56] Rabeti SAM, Manesh MHK, Amidpour M. Optimal 4E Design and Innovative R-Curve Approach for a Gas-Solar-Biological Waste Polygeneration System for Power, Freshwater, and Methanol Production. Process Saf Environ Prot 2024;191:1254–77.
[57] Manesh MHK, Davadgaran S, Rabeti SAM. Gasification potential of municipal solid waste in Iran: Application of life cycle assessment, risk analysis, and machine learning. J Clean Prod 2024;434:140177.
[58] Ghasemzadeh N, et al. Thermodynamics modeling and optimisation of a biogas fueled decentralised poly-generation system using machine learning techniques. Energy Conversion and Management: X 2023;20:100470.
[59] Ghandehariun S, Ghandehariun AM, Ziabari NB. Performance prediction and optimization of a hybrid renewable-energy-based multigeneration system using machine learning. Energy 2023;282:128908.
[60] Dincer I, Rosen MA, Ahmadi P. Optimization of energy systems. John Wiley & Sons; 2017.
[61] Georgousis N, et al. Multi-objective optimization of a solar-driven polygeneration system based on CO2 working fluid. Energy Convers Manag 2022;252:115136.
[62] Teichgraeber H, Brandt AR. Clustering methods to find representative periods for the optimization of energy systems: An initial framework and comparison. Appl Energy 2019;239:1283–93.
[63] Mahmoud FS, et al. Optimal sizing of smart hybrid renewable energy system using different optimization algorithms. Energy Rep 2022;8:4935–56.
[64] Liu L, Zhai R, Hu Y. Multi-objective optimization with advanced exergy analysis of a wind-solar-hydrogen multi-energy supply system. Appl Energy 2023;348:121512.
[65] Mahmoudan A, et al. A geothermal and solar-based multigeneration system integrated with a TEG unit: Development, 3E analyses, and multi-objective optimization. Appl Energy 2022;308:118399.
[66] Assareh E, et al. Optimizing solar photovoltaic farm-based cogeneration systems with artificial intelligence (AI) and Cascade compressed air energy storage for stable power generation and peak shaving: A Japan-focused case study. Appl Energy 2025;377:124468.
[67] Manesh MHK, Davadgaran S, Rabeti SAM. Novel Solar-Biomass polygeneration system based on integration of ICE-ORC-MDC-HDH-RO and tomato greenhouse to produce power, freshwater, and biological wastewater treatment. Energy Convers Manag 2024;308:118349.
[68] Alamdari P, Nematollahi O, Mirhosseini M. Assessment of wind energy in Iran: A review. Renew Sust Energ Rev 2012;16(1):836–60.
[69] Tzivanidis C, Bellos E, Antonopoulos KA. Energetic and financial investigation of a stand-alone solar-thermal Organic Rankine Cycle power plant. Energy Convers Manag 2016;126:421–33.
[70] Ishaq H, Dincer I. A novel biomass gasification based cascaded hydrogen and ammonia synthesis system using Stoichiometric and Gibbs reactors. Biomass Bioenergy 2021;145:105929.
[71] Ishaq H, et al. Development and performance investigation of a biomass gasification based integrated system with thermoelectric generators. J Clean Prod 2020;256:120625.
[72] Makkeh SA, et al. Energy, exergy and exergoeconomic optimization of a cogeneration system integrated with parabolic trough collector-wind turbine with desalination. J Clean Prod 2020;273:123122.
[73] MOUSAZADE, M.R., et al., Mathematical Modeling of Waste Engine Oil Gasification for Synthesis Gas Production; Operating Parameters and Simulation. International Journal of Thermodynamics: p. 1–13.
[74] Ahmadi P, Dincer I, Rosen MA. Energy and exergy analyses of hydrogen production via solar-boosted ocean thermal energy conversion and PEM electrolysis. Int J Hydrog Energy 2013;38(4):1795–805.
[75] Kim MS, et al. Study on the supercritical CO2 power cycles for landfill gas firing gas turbine bottoming cycle. Energy 2016;111:893–909.
[76] Yari M. Exergetic analysis of various types of geothermal power plants. Renew Energy 2010;35(1):112–21.
[77] Zupančič J, Filipič B, Gams M. Genetic-programming-based multi-objective optimization of strategies for home energy-management systems. Energy 2020;203:117769.
[78] Noorbakhsh H, Manesh MHK, Amidpour M. Evaluation of an innovative polygeneration system based on integration of gasification process with a thermo electric generator-solid oxide fuel cell-Adsorption desalination system-Thermal photovoltaic collector. Energy 2023;282:128672.
[79] Yilmaz, F., M. Ozturk, and R. Selbas, Thermodynamic investigation of a concentrating solar collector based combined plant for poly-generation. Int J Hydrog Energy, 2020. 45(49): p. 26138–26,155.
[80] Hosseini M, Dincer I, Rosen MA. Hybrid solar–fuel cell combined heat and power systems for residential applications: Energy and exergy analyses. J Power Sources 2013;221:372–80.
[81] Elsafi AM. Exergy and exergoeconomic analysis of sustainable direct steam generation solar power plants. Energy Convers Manag 2015;103:338–47.
[82] Kotas TJ. The exergy method of thermal plant analysis. Paragon Publishing; 2012.
[83] Manesh MK, et al. Energy, exergy, exergoeconomic, and exergoenvironmental analysis of an innovative solar-geothermal-gas driven polygeneration system for combined power, hydrogen, hot water, and freshwater production. Sustain Energy Technol Assessments 2022;51:101861.
[84] Ptasinski KJ, Prins MJ, Pierik A. Exergetic evaluation of biomass gasification. Energy 2007;32(4):568–74.
[85] Cavalcanti EJC. Exergoeconomic and exergoenvironmental analyses of an integrated solar combined cycle system. Renew Sust Energ Rev 2017;67:507–19.
[86] Chau CK, Leung T, Ng W. A review on life cycle assessment, life cycle energy assessment and life cycle carbon emissions assessment on buildings. Appl Energy 2015;143:395–413.
[87] Meyer L, et al. Exergoenvironmental analysis for evaluation of the environmental impact of energy conversion systems. Energy 2009;34(1):75–89.
[88] Shamsi M, et al. Evaluation of an environmentally-friendly poly-generation system driven by geothermal energy for green ammonia production. Fuel 2024;365:131037.
[89] Xing L, Li J. Proposal of biomass/geothermal hybrid driven poly-generation plant centering cooling, heating, power, and hydrogen production with CO2 capturing: Design and 3E evaluation. Fuel 2022;330:125593.
[90] Xu C, et al. Thermodynamic analysis of a novel biomass polygeneration system for ammonia synthesis and power generation using Allam power cycle. Energy Convers Manag 2021;247:114746.
[91] Ansari SA, et al. Thermal analysis of multigeneration system using geothermal energy as its main power source. Int J Hydrog Energy 2021;46(6):4724–38.
[92] Demir ME, Dincer I. Development and assessment of a solar driven trigeneration system with storage for electricity, ammonia and fresh water production. Energy Convers Manag 2021;245:114585.
[93] Luqman M, Bicer Y, Al-Ansari T. Thermodynamic analysis of an oxy-hydrogen combustor supported solar and wind energy-based sustainable polygeneration system for remote locations. Int J Hydrog Energy 2020;45(5):3470–83.
[94] Mirjalili S. Dragonfly algorithm: a new meta-heuristic optimization technique for solving single-objective, discrete, and multi-objective problems. Neural Comput & Applic 2016;27(4):1053–73.
[95] Ameri M, Ahmadi P, Hamidi A. Energy, exergy and exergoeconomic analysis of a steam power plant: A case study. Int J Energy Res 2009;33(5):499–512.
[96] Habibollahzade A, Gholamian E, Behzadi A. Multi-objective optimization and comparative performance analysis of hybrid biomass-based solid oxide fuel cell/solid oxide electrolyzer cell/gas turbine using different gasification agents. Appl Energy 2019;233:985–1002.
[97] Bonyadi N, Johnson E, Baker D. Technoeconomic and exergy analysis of a solar geothermal hybrid electric power plant using a novel combined cycle. Energy Convers Manag 2018;156:542–54.
[98] Nami H, Mahmoudi S, Nemati A. Exergy, economic and environmental impact assessment and optimization of a novel cogeneration system including a gas turbine, a supercritical CO2 and an organic Rankine cycle (GT-HRSG/SCO2). Appl Therm Eng 2017;110:1315–30.
[99] Lüpfert, E., et al. Euro Trough collector qualification complete-performance test results from PSA. in ISES Solar World Congress 2001 & 2003 Proceedings 2003.
[100] Kabiri S, Khoshgoftar Manesh MH, Amidpour M. 4E analysis and evaluation of a steam power plant full repowering in various operations. Energy Sources, Part A: Recovery, Utilization, and Environmental Effects 2020:1–21.
[101] Nami, H., F. Ranjbar, and M. Yari, Methanol synthesis from renewable H2 and captured CO2 from S-Graz cycle–Energy, exergy, exergoeconomic and exergoenvironmental (4E) analysis. Int J Hydrog Energy, 2019. 44(48): p. 26128–26,147.
[102] Ansarinasab H, Mehrpooya M, Sadeghzadeh M. Life-cycle assessment (LCA) and techno-economic analysis of a biomass-based biorefinery. J Therm Anal Calorim 2021;145(3):1053–73.
[103] Jadidi E, et al. Advanced Exergy, Exergoeconomic, and Exergoenvironmental Analyses of Integrated Solar-Assisted Gasification Cycle for Producing Power and Steam from Heavy Refinery Fuels. Energies 2021;14(24):8409.